University of Puerto Rico
Faculty of Natural Sciences
Department of Chemistry
Río Piedras Campus

Intracellularly Dissolving Chromophore-decorated Protein-based Nanoparticles for Photodynamic Cancer Therapy

A Dissertation Submitted in Partial
Fulfillment of the Requirements
for the Degree of Doctor in Philosophy

By
Anna M. Molina Calzada
July 2016

This dissertation has been accepted by
the faculty of the

Natural Sciences
Chemistry Department
Río Piedras Campus
University of Puerto Rico

In partial fulfillment of the requirements
For the degree of

DOCTOR IN PHILOSOPHY

In the subject of
CHEMISTRY

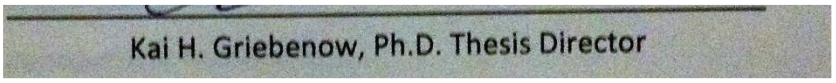

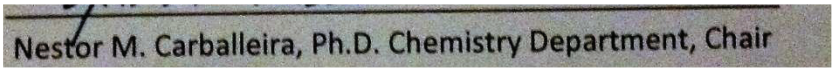

Table of Contents

Tables captions

Chapter 1

Chapter 3

Chapter 4

Figures captions

Chapter 1

Chapter 4

Abbreviations

Apaf-1	Apoptotic protease activating factor 1
CD	Circular Dichroism
Ce6	Chlorin e6
Cyt c	Cytochrome c
DAPI	4',6-diamidino-2-phenylindole
DDS	Drug Delivery System
DLS	Dynamic Light Scattering
DNA	Deoxyribonucleic acid
DSP	Dithiobis(succinimidyl propionate)
DTT	Dithiothreitol
EDC	1-ethyl-3-(-3-dimethylaminopropyl) carbodiimide hydrochloride
EDTA	Ethylenediaminetetraacetic acid
EPR	Enhance Permeability and Retention Effect
FBS	Fetal Bovine Serum
FDA	Food and Drug Administration
FITC	Fluorescein isothiocyanate
GHS	Glutathione
HeLa	Cervical cancer human cell line
HSA	Human Serum Albumin
MES	4-Morpholineethanesulfonic acid sodium salt
MEM	Minimum Essential Media
NHS	N-Hydroxysuccinimide
NP	Nanoparticle
PBS	Phosphate Buffer Saline
PDT	Photodynamic therapy
PEG	Poly-ethylene glycol
PI	Propidium Iodide
PS	Photosensitizer
RES	Reticuloendothelial system
SEM	Scanning Electron Microscopy
UV-Vis	Ultraviolet/Visible

Abstract

Cancer has proven to be extremely complex to treat and cure due to its heterogeneity. Current treatments rely mainly on chemotherapeutic drugs, which typically result in multidrug resistance and the generation of additional genetic mutations. In this context, protein-based therapeutics are a promising alternative. In general, proteins are natural and biocompatible macromolecules with highly specific biological activities. However, their physical and chemical instability make their formulation, storage and delivery very challenging. The emerging field of engineering nano-sized delivery systems provides exciting new opportunities to formulate proteins into nanoparticles. In this dissertation, intracellularly dissolvable protein-based nanoparticles are used as carrier for photosensitizer drugs. Photosensitizers induce cell death after irradiation by the generation of reactive oxygen species in a treatment known as photodynamic therapy (PDT).

In *Chapter 3*, the redox-sensitive albumin nanoparticles for the delivery of the photosensitizer drug Chlorin e6 (Ce6) is systematically studied. The reversible inactivation of Ce6 as a consequence of immobilization on the nanoparticle surface was evidenced. Furthermore, its activation upon the nanoparticle dissolution in a reducing environment, such as the cell interior, was evaluated. *In vitro* experiments show that the synthesized redox-sensitive system enhances the function of albumin nanoparticles as carriers for photosensitizer drugs, as it prevents phototoxicity during delivery, and allows for drug activation only after cell uptake.

In *Chapter 4*, the redox-sensitive protein-based nanoparticles are prepared with Cytochrome c (Cyt c), a pro apoptotic protein, and decorated with Ce6 for low-dose PDT. Low dose PDT has been associated with the induction of apoptosis whereas high dose PDT is associated with the induction of necrosis, a type of cell death that produces inflammation and affects neighboring tissue. The experimental results show that, upon modification, the Cyt c loses some of its pro apoptotic activity, but that a high level of function can be retained at a low drug:protein ratio. Additionally, *in vitro* experiments results showed that the protein nanoparticles were internalized by the cells, even without the use of a targeting moiety. The combination of both therapeutic agents into a single nanoparticle allowed for a greater induction of cell death. Evidence showed that the death induced was via apoptosis instead of necrosis.

Author's biography

Anna M. Molina Calzada was born in San Juan, Puerto Rico, on September 23, 1987. She is the third child of her parents, Sandra E. Calzada and Eddie Molina. Her older sisters are Marla and Carla Molina Calzada. Anna grew up with her family in Canóvanas, PR, where she completed her education up until high school. She graduated with honors from Luis Hernaiz Veronne School in Canóvanas and was the recipient of the National Hispanic Scholar Award for her outstanding score in the College Board. She received early admission to the University of Puerto Rico in Rio Piedras to study Chemistry. She started doing undergraduate research right after her freshman year, and made scientific research her professional goal. Anna worked for three years in the Environmental Analytical Research Laboratory of Dr. Osvaldo Rosario. Her research focused on the development of analytical methods to detect trace amounts of pharmaceutical compounds in the natural waters of Puerto Rico. She was a RISE and a NASA Space Grant fellow, and participated in two undergraduate research internships. At the Cornell Center for Materials Research in Cornell University, she conducted nanofiber science research for the detection of volatile organic compounds in air under the mentoring of Dr. Margaret Frey in the summer of 2007. The following year, she went to Texas A&M University to conduct research on the nighttime formation of radical Nitrogen oxide species under the mentoring of Dr. Simon North. As an undergraduate she was the recipient of several awards, including the Natural Sciences Dean Honor Roll, the ABRCMS outstanding poster presentation award, and the Joseph Axthmayer award, conferred to the highest GPA in Chemistry.

In 2010, Anna was admitted to the Chemistry Graduate Program. She approved her qualifying exams on the summer of 2011, and started working in the Biochemistry and Applied Biotechnology Laboratory under the mentoring of Dr. Kai Griebenow. The focus of this research laboratory is the biophysical study of proteins for different applications and the design and development of protein-based and polymeric drug delivery systems for cancer therapy. Anna did some work on biophysical studies of chemically glycosylated proteins and later focused on drug delivery systems for cancer therapy. Her research thesis proposal was approved in 2013, and the first part of her thesis work was published in 2015. Anna is the author/coauthor of five peer-reviewed publications.

During her graduate studies, Anna participated in numerous conferences in Puerto Rico and the US, and was the recipient of the NASA CAMN, RISE and IFN fellowships. In the academic year 2014-2015, Anna served as the student representative of the Graduate Chemistry Department. In September of 2015, she co-founded and became the first president of the Asociación Graduada de Química. She also participated in an internship experience in a Technical Services/Manufacturing Sciences laboratory at Lilly del Caribe as part of the program Mi Primera Experiencia Laboral.

Anna is married to Samuel E. Ramírez and has a child, Esteban Ramírez.

Peer-reviewed publications

Morales-Cruz, Moraima; Cruz-Montañez, Alejandra; Figueroa, Cindy; Gonzalez-Robles, Tania; Davila, Josue; Inyushin, Mikhail; Loza-Rosas, Sergio; **Molina, Anna**; Muñoz-Perez, Laura; Kucheryavykh, Lilia; Tinoco, Arthur; Griebenow, Kai. Combining stimulus-triggered release and active targeting strategies improves cytotoxicity of cytochrome c nanoparticles in tumor cells. *Molecular Pharmaceutics*, 2016. Just Accepted Manuscript.

Cindy M Figueroa, Moraima Morales-Cruz, Bethzaida N Suárez, Jean C Fernández, **Anna M Molina**, Carmen M Quiñones and Kai Griebenow. Induction of Cancer Cell Death by Hyaluronic Acid-Mediated Uptake of Cytochrome C. *Journal of Nanomedicine and Nanotechnology*, Volume 6, Number 316. October 2015.

Anna M Molina, Moraima Morales-Cruz, Marimar Benítez, Kiara Berríos, Cindy M Figueroa, Kai Griebenow. Redox-Sensitive Cross-Linking Enhances Albumin Nanoparticle Function as Delivery System for Photodynamic Cancer Therapy. *Journal of Nanomedicine and Nanotechnology*, Volume 6, Number 294. May 2015.

Moraima Morales-Cruz, Cindy M Figueroa, Tania González-Robles, Yamixa Delgado, **Anna Molina**, Jessica Méndez, Myraida Morales, Kai Griebenow. Activation of caspase-dependent apoptosis by intracellular delivery of cytochrome c-based nanoparticles. *Journal of Nanobiotechnology*, Research Article, Volume 12, Number 33, September 2014.

Liz M. Díaz-Vázquez, Bárbara Casañas Montes, Ileabett Echevarría Vargas, Griselle Hernández, Fernando González Illán, **Anna Molina-Calzada**, Moraima Morales-Cruz, Carlos Torres-Díaz, and Kai Griebenow. An Investigative Cooperative Learning Approach for General Chemistry Laboratories, *International Journal for the Scholarship of Teaching and Learning*, Research Article, Volume 6, Number 2, July 2012.

Dedication

I dedicate this work to the patients battling cancer and to the scientists whose creativity and hard work have brought new therapies to the clinic. I also dedicate it to my loving husband Samuel, my son Esteban, and my mother Sandra who supported me throughout this long career.

Acknowledgments

Many people have contributed to the successful completion of my PhD degree. I owe a great debt of gratitude to my PI, Prof. Kai Griebenow, for guiding and mentoring me in my research. I especially enjoyed the company, friendship, and support of my labmates thoughout my studies. Cindy, Moraima, Yamixa, Zally, Freisa (the Covacha girls): I will *really* miss working with you. Many thanks to the undergraduate students that collaborated with me and did an excellent job: Kiara Berríos and Marimar Benítez. I expect great things form you.

I also acknowledge the great contribution of Bismark Madera from the Confocal Imaging Facility, and Cristina Díaz-Borrero, Lorraine Soto-Vázquez, and Julia Medina from the Scanning Electron Microscopy Facility for their technical assistance.

I am very thankful for the members of my thesis committee. Prof. Rosario introduced me to scientific research and inspired me to continue. I also recognize Prof. Liz Díaz, who has been extremely helpful and supportive throughout my career, and Prof. Arthur Tinoco for his disposition to help and provide useful feedback. I also thank the administrative personnel of the Graduate Chemistry Department, and Prof. Jorge Colón, the Program coordinator, for his continuous support.

I am very grateful for Adolfo Plazaola and Lilly del Caribe for giving me the opportunity of working with them during a semester. Many thanks to Vladimir Vélez, and the rest of the team at the Technical Services/Process Development laboratory.

Many thanks to my family for their love and encouragement.

Chapter 1

Introduction

1.1 Protein-based therapeutics

Proteins are natural complex macromolecules that perform catalytic, regulatory, and transport functions, among many others [Alberts et al., 2014]. Their biocompatibility and their substrate specificity make them an attractive biotechnological and clinical tool. Protein-based therapeutics are now being extensively investigated and used for the treatment of a range of diseases. Recombinant DNA technology, the method that makes possible to obtain large quantities of proteins, uses mainly bacteria such as *Escherichia coli* as expression systems [Rosano and Ceccarelli, 2014]. The first recombinant therapeutic protein to reach the market, a genetically engineered insulin by Eli Lilly & Company, was approved by the FDA in 1982. Today, nearly 170 proteins and peptides obtained from recombinant DNA technology are approved and in use for the therapy of cancers, immune disorders, infections, and other diseases. Recombinant proteins accounted for sales worth $37 billion in 2003, and achieved a whopping $90 billion in 2010, approximately 14% of the global pharmaceutical market. Much of this market is dominated by erythropoietin and monoclonal antibodies, which treat common diseases such as anemia, arthritis and cancer [Leader et al., 2008; Dimitrov, 2012].

In earlier years, protein therapeutics were dominated by structures based on naturally-occurring, native sequences. Later, additional features were pursued, including enhanced biodistribution, specificity, efficacy and reduced side effects (Table 1.1). Protein sequence changes, glycosylation, covalent modification, and fusion of two or

Table 1.1 FDA approved protein therapeutics. Examples of first generation proteins (based on native structures), and second generation (modified proteins), shaded gray

Brand	Generic	Company	Therapeutic category	Disease
Humilin	Insulin	Eli Lilly	Diabetes	Diabetes
Genotropin	Somatropin	Pfizer	Hormone	Growth failure
Avonex	Interferon-beta-1a	Biogen Idec	Multiple sclerosis	Chronic inflammatory demyelinating polyneuropathy
Epogen	Epoetin alpha	Amgen	Blood modifier	Anemia
Pulmozyme	Dornase alpha	Genentech	Enzyme	Cystic fibrosis
Activase	Alteplase	Genentech	Blood factor	Myocardial infarction
Humalog	Insulin lispro	Eli Lilly	Diabetes	Diabetes
Lantus	Glargine insulin	Sanofi-Aventis	Diabetes	Diabetes
Pegasys	Pegylated interferon alpha-2a	Roche	Interferon	Hepatitis C
Aranesp	Darbepoetin alpha	Amgen	Blood modifier	Anemia
Neulasta	PEG-Filgrastim	Amgen	Blood modifier	Neutropenia
ReFacto	Factor VIII	Wyeth	Blood modifier	Hemophilia
Amevive	Alefacept	Biogen Idec.	Inflammation/Bone	Plaque psoriasis
Enbrel	Etanercept	Amgen	Anti-arthritic	Arthritis
Ontak	rIL-2-diphteria toxin	Ligand Pharmaceuticals	Cancer	Cancer

more peptide chains are the most common modifications. Some of these modifications aim at preserving the protein's structure and function during storage and delivery. However, these types of complexes are mostly limited to cell surface or extracellular targets *in vivo* [Carter, 2011].

For some applications, protein-based bioconjugates have been formulated into nanoparticles and other nano-sized constructs. Albumin, transferrin, gelatin, and antibodies are some of the most common proteins used to build these complexes, as well as peptides such as RGD and cell penetrating peptides [Vhora et al., 2015]. The formulation of proteins into larger, more complex constructs for their delivery can potentially make them more viable as therapeutic tools. Protein delivery systems can protect their structure and activity during delivery, as well as enhance its targeting capabilities. As discussed later, the proteins in nanoparticles can serve both as the therapeutic agent and as the carrier for small drugs.

1.2 Nanoparticles in cancer therapeutics

Nanoparticles as a therapeutic strategy for many diseases have been explored extensively in the past few decades. They have emerged as an approach to improve drug stability, solubility and selectivity towards target tissue [Sun et al., 2014]. Recently, nanotechnology has had a special role in the development of treatments for cancer.

Cancer is a heterogeneous group of diseases that are caused by the uncontrolled proliferation of abnormal cells that have a malignant behavior. Malignant cells can inva-

de the surrounding tissue and cause metastasis. Cancer types are classified depending on their behavior, appearance and origin. Even though it is the center of much research, cancer is still one of the most challenging diseases to fight in the clinic.

The most common treatments for cancer currently include chemotherapy by the administration of mitotic inhibitory drugs, radiotherapy and surgery. Chemotherapy remains the pillar of cancer treatment, but has the inherent drawback of lack of specificity, and is susceptible to failure due to multidrug resistance [Housman et al., 2014; Hanahan and Weinberg, 2011].

The incorporation of chemotherapeutic drugs into drug delivery systems (DDS), mostly nanoparticles and liposomes, have helped increase their specificity and pharmacokinetic profile, hence reducing the undesirable side effects typically associated with chemotherapy. Many nano-sized therapeutic agents have shown efficacy in animal cancer models, and several are currently undergoing testing in clinical trials [Kano et al., 2007; Riggio et al., 2011]. Some of these DDS have even reached the clinic for several types of cancer, including liposomal formulations and polymeric nanoparticles (Table 1.2). The development of effective nano-sized DDS relies on identifying the differences between the healthy and the cancerous tissue.

1.3 Targeting of tumor microenvironment

Tumor tissue and its microenvironment exhibit specific characteristics that make them different from healthy tissue. Cancer cells sustain proliferation by deregulating the growth control mechanisms, evading apoptosis, and inducing angiogenesis [Hanahan

Table 1.2 FDA approved nanoparticle based therapeutic agents for the treatment of cancer

Brand name	Nano-platform	Approved for	Company	References
Doxil	Liposomal-polyethylene glycol doxorubicin	HIV-related Kaposi's sarcoma, metastatic breast cancer, and metastatic ovarian cancer	Ortho Biotech, Schering-Plough	Duggan and Keating, 2011
DaunoXome	Liposomal daunorubicin	HIV-related Kaposi's sarcoma	Gilead	Petre and Dittmer, 2007
Oncaspar	Polyethylene glycol-L-Asparaginase	Acute lymphoblastic leukemia	Enzon	Dinndorf et al., 2007
Abraxane	Albumin-bound paclitaxel	Metastatic breast cancer	Astra-Zeneca	Miele et al., 2009
OncoTCS	Liposomal Vincristine	Relapsed aggressive non-Hodgkin's lymphoma	Enzon/INEX	Raj et al., 2013
Genexol-PM	Methoxy-PEG-poly(D, L-lactide) paclitaxel	Metastatic breast cancer	Samyang	Lee et al., 2008
Myocet	Liposomal doxorubicin	Metastatic breast cancer (In combination with cyclophosphamide)	Zeneus	Elbayoumi, T. A. and Torchilin, V. P, 2008

and Weinberg, 2010]. The rapid and abnormal proliferation of cells induce other changes in the tumor microenvironment. The vasculature that surrounds the tumor is leaky, and the lymphatic drainage is poor compared with healthy vessels in normal organs [Danhier et al., 2010]. This allows for large molecules and particles to enter the irregular tumor fenestrae. This phenomenon is known as the Enhanced Permeability and Retention (EPR) effect [Greish, 2010; Maeda, 2012] (Figure 1.1).

Nanoparticles and macromolecular bioconjugates can take advantage of this effect if they are within a specific size range. Particles from 100 to 800 nm can penetrate the abnormally permeable vasculature due to the larger size of gap junctions between the endothelial cells and be retained. However, they must be bigger than 20 nm to avoid renal filtration during circulation [Torchilin, 2011; Schroeder et al., 2011]. Additionally, they should be invisible to the macrophage phagocytic system to avoid their clearance and be able to circulate for prolonged times when administered intravenously [Kobayashi and Brechbiel, 2005]. Using the size characteristics to target the tumor tissue is known as *passive targeting*, as it relies on the accumulation by diffusion of the nano-sized therapeutic agents into the tumor bed. The EPR effect alone increases the nano-sized DDS tumor specificity by 20-30% over critical normal organs [Kobayashi et al., 2014]. Therefore, the EPR effect is an important factor to be considered in the design of potential DDS for the treatment of cancer. Its combination with additional targeting strategies, such as modifications with ligands to overexpressed cell-surface receptors, can potentially result in much more powerful therapies.

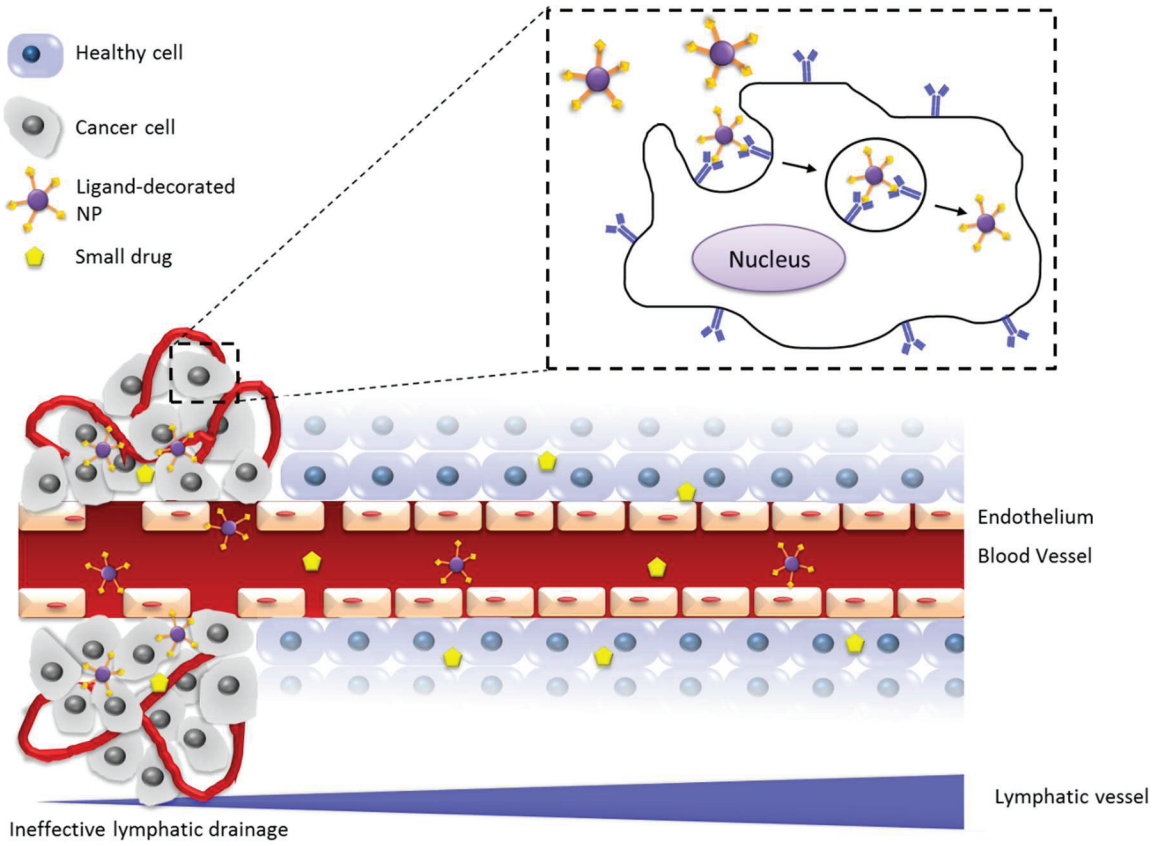

Figure 1.1 Scheme of *passive targeting* via enhanced permeability and retention (EPR) effect. While small drugs can efficiently penetrate both healthy tissue and tumor tissue, nanoparticle-based DDS permeate preferentially into tumor tissues through its leaky tumor vasculature. Additionally, they are retained due to the tumor lack of efficient lymphatic drainage. Decorating the nanoparticles with targeting ligands allows for specific or preferential binding to tumor cells followed by receptor-mediated endocytosis. This type of targeting is known as *active targeting*. The therapeutic component can be released in the extracellular environment or inside the cell after endocytic uptake.

The particle size is not the only characteristic that should be taken into account when designing new DDS. Previous research has shown that other features may improve DDS blood-half time and tumor cell uptake. The particle surface charge can affect its interaction with the vascular endothelial luminal surface. For instance, hydrophobic or negatively charged nanoparticles have shown fast uptake by the macrophage phagocytic system in the liver and spleen. To protect nanoparticles from the RES, the most commonly used strategy is to conjugate poly(ethylene glycol) (PEG) onto the nanoparticle surface to cover any undesired charge or surface properties [Fang et al., 2011; Narang and Varia, 2011]. Extensive characterization of new DDS properties is necessary to predict how it will interact with the organism.

Once the DDS has successfully reached the tumor vicinity, it needs to be internalized in order to release its drug payload inside of the cell. A very effective way of enhancing targeted cell uptake is by the DDS modification with ligands that are overexpressed in the tumor cells, but not on healthy cells [Torchilin, 2011; Fang et al., 2011; Jaracz et al., 2005]. Targeting moieties for molecular recognition (e.g. ligand of a receptor, antibodies, and aptamers) can de directly grafted onto the particle surface. This targeting strategy is known as *active targeting* (Figure 1.1). Active targeting allows for specific retention and uptake of nanoparticles in the cell vicinity mediated by surface receptors. The ligands include antibodies, peptides, and small molecules. Also, factors such as ligand density and nanoparticle size affect its avidity for its target [Bertrand et al., 2013]. Since active targeting cannot significantly alter nanoparticle biodistribution, the

use of passive targeting together with active targeting can lead to better cancer therapeutics.

1.4 Stimulus-responsive delivery

An additional tumor targeting strategy takes advantage of specific characteristics of the chemical environments of tumor interstitium or the cell interior. It depends on an extracellular, intracellular, or external stimulus that triggers drug release or activation. Such stimuli include pH, protease and redox-sensitivity, heat, light, among others [Torchilin, 2014].

Since many cancer cells generate energy exclusively by glycolysis and are generally deprived of oxygen, the extracellular matrix of tumor sites frequently have a lower pH compared to normal tissue, ranging from 5.5 to 7.0. Also, it is rich in proteases. These characteristics have encouraged, for example, the design of pH-sensitive liposomes and polymeric micelles [Karanth et al., 2007, Liu et al., 2013], as well as protease-sensitive DDS [Choi et al., 2012].

Differences in the reducing potential between the extra- and intra-cellular spaces provide another opportunity. The cell cytoplasm is significantly more reducing than the outside of the cell, with a concentration of reducing species, mainly glutathione (GHS), as much as 1000 times higher [Lushchak, 2012]. DDS that are redox-activated will exhibit intracellular drug release or activation [Hong et al., 2006]. Therefore, they would only be cytotoxic to the cells that internalize them. Redox-responsive DDS can be generated by using thiol-cleavable crosslinkers, which will break down upon reduction by GHS. Such systems have been used to trigger the release of pro-apoptotic proteins in the cell

cytoplasm [Méndez et al., 2012; Zhao et al., 2011]. When used in combination with passive and/or active targeting, these stimuli-responsive strategies can potentially significantly enhance the DDS selectivity towards cancer tissue and overall therapeutic index. In this dissertation, we evaluate redox-responsiveness as targeting strategy.

1.5 Albumin as a carrier for drug delivery formulations

Human serum albumin (HSA) is the most abundant protein in human plasma and plays a determinant role in the osmotic balance and the transport of many metabolic compounds and drugs. This resilient protein remains stable over a pH range of 4-9 and at high temperatures (60°C). It is readily available, biodegradable, has a long blood half-life, and low immunogenicity. These characteristics make it a very attractive candidate to be used as a drug carrier [Kratz, 2008]. HSA has been formulated into nanoparticles to be used as DDS by robust and well-characterized methods [Gallo et al., 1984; Lin et al., 1993; Muller et al., 1996; Langer et al., 2003]. Gallo, et al. [1984] used an emulsion technique to prepare HSA microspheres and optimized the synthesis conditions. Müller, et al. [1996] used a similar method to synthesize bovine serum albumin (BSA) nanoparticles under 200 nm. Lin, et al. [1993] described the pH-coacervation method to produce surfactant-free nanoparticles between pH 7 and 9 and found that a higher pH favored the formation of smaller particles due to charge repulsions caused by higher ionization. Even though the obtained size range was desirable (90-250 nm), a broad size distribution was observed. Langer et al. [2003] optimized the desolvation procedure to obtain a narrow sized distribution. The desolvation technique or solvent displacement developed consists of the following steps: the protein is dissolved in an aqueous solution at a high concentration,

titrated to the desired pH, and the desolvating agent is added at a constant rate to the solution under stirring at room temperature. Finally, a crosslinker is added to the suspension and incubated under stirring to obtain protein nanoparticles that do not dissolve in aqueous media.

Apart from its many desirable characteristics, albumin has been found to accumulate preferentially in tumor and inflamed tissue, a property being exploited in the FDA-approved anti-cancer drug Abraxane® (Albumin-bound paclitaxel nanoparticles). The albumin in Abraxane targets the Gp60 receptor, overexpressed in a majority of tumors, to enhance the intra-tumoral concentrations of paclitaxel by endothelial transcytosis [Desai, 2007; Pillai, 2014]. Hence, Abraxane uses albumin as an active targeting tool.

1.6 Other protein-based nanoparticles

A number of protein-, antibody-, and peptide-drug conjugates have been synthesized and tested. Albumin and transferrin have been extensively used as carriers because they improve pharmacokinetics and also target their overexpressed receptors in some cancer types [Yousefpour and Chilkoti, 2014]. Humanized antibodies carry out the same function, while enhancing cell specific uptake; ADCs being the most explored antibodies [Wang et al., 2008]. Other proteins and cell penetrating peptides are used based on their interaction with specific cell types [Zahid and Robbins, 2015]. However, proteins in nanoparticles and other nano-complexes can do more than providing a vehicle for drugs and targeting moieties. They can also be a therapeutic agent in the formulation. Because of the proteins biocompatibility and biodegradability, they are an attractive substitute of cytotoxic drugs. In the particular case of cancer, therapeutic proteins are far

superior than chemotherapy drugs, which cause additional mutations and lead to multidrug resistance. In this dissertation we use C*ytochrome c*, a pro-apoptotic protein, as a therapeutic agent.

Cytochrome c (Cyt c) is a natural protein that mediates apoptosis by its release from the mitochondria to the cytoplasm. Apoptosis is a highly regulated form of programmed cell death characterized by defined morphological changes, including cell shrinkage, chromatin condensation, and plasma membrane blebbing [Elmore, 2007]. In cells that are not apoptotic, Cyt c is located in the intermembrane space of the mitochondria [Gillick and Crompton, 2008]. Upon apoptotic stimulus, it leaks out to the cytoplasm to bind the apoptotic protease activating factor 1 (Apaf-1) and form a protein complex known as the apoptosome [Zhou et al., 2015]. This results in the activation of the caspase cascade unleashing apoptosis (Figure 1.2).

The process of apoptosis occurs normally in cells as a response to DNA damage, and is part of the normal cell cycle. However, in many cancer cells apoptosis is inhibited. The p53 transcription factor, encoded by the human gene TP53, has tumor suppressor functions and modulates cell cycle, DNA repair, senescence, and apoptosis, among other processes [Aylon and Oren, 2011]. Evidence shows that TP53 mutations occur in almost every type of cancer, ranging from 10 to 100% of malignancies [Ahmed et al., 2010]. Apart from losing their tumor suppressive capabilities, cells with mutant p53 typically gain oncogenic functions that favor tumor initiation, and eventual metastasis [Rivlin et al., 2010]. The release of the Cyt c from the mitochondria is a process that occurs downstream

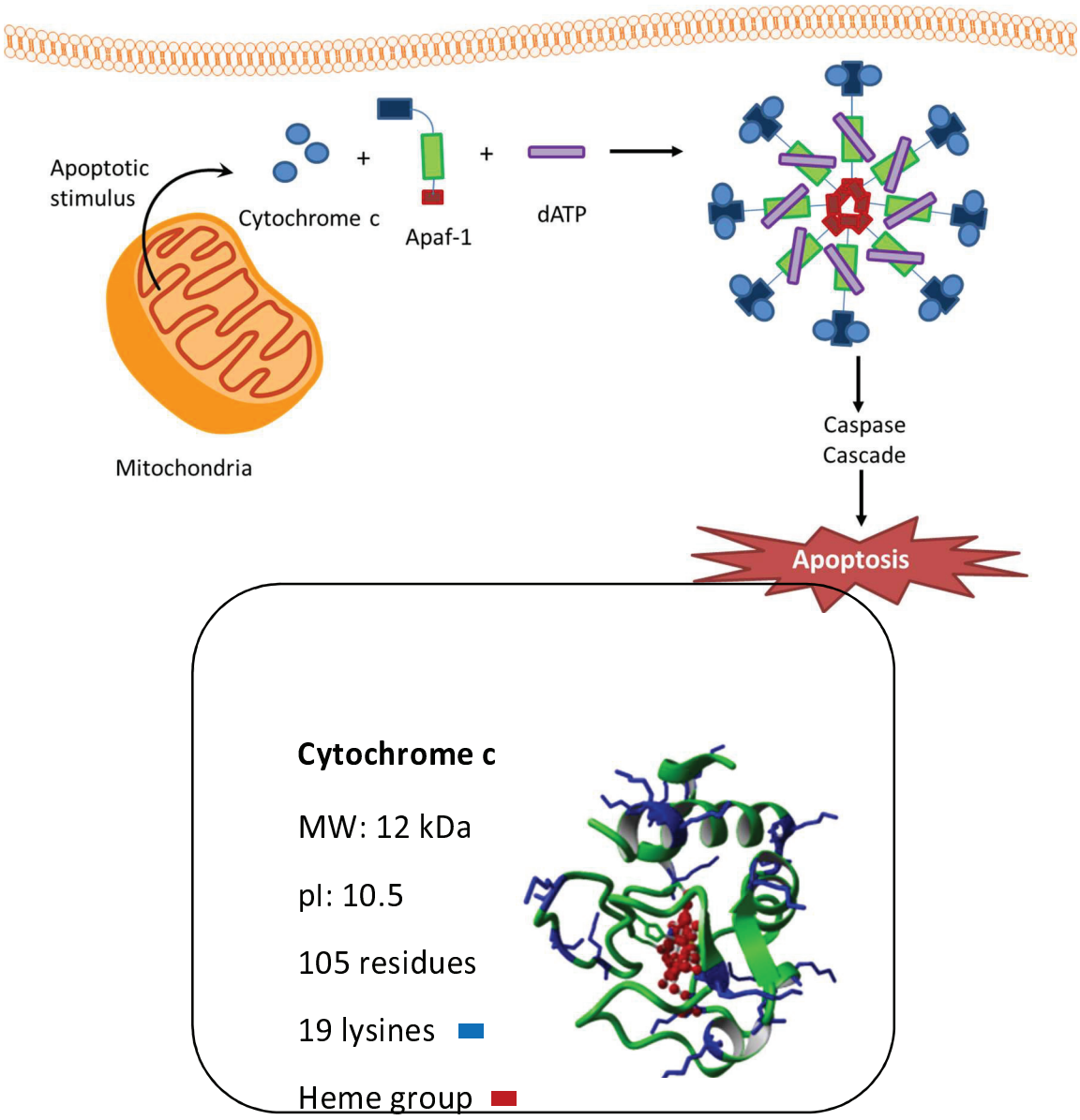

Figure 1.2 Schematic representation of Cytochrome c-mediated apoptosis pathway. Upon apoptotic stimulus, cytochrome c is released from the mitochondria intermembrane space to the cell cytoplasm. There it interacts with Apaf-1 to form the apoptosome, which activates caspase-9 and a series of effector caspases, including caspase-3 and -7, that lead to apoptosis. The cytochrome c molecular structure is shown below.

to p53 activity, so direct delivery of Cyt c to the cell cytoplasm can effectively induce apoptosis in cells with p53 mutations.

1.7 Protein nanoparticle formulation

As water soluble molecules, proteins formulated into nanoparticles must be stabilized through covalent crosslinking or coating with amphiphilic molecules. Since proteins have many functional groups, there are many ways in which they can be chemically modified. The protein modification strategies for stabilization must consider the preservation of the protein activity and structure. Therefore, the reaction conditions should not be harsh (e.g. solvents, pH, etc.). Also, the selected amino acids for the conjugation of drugs, ligands or crosslinkers should be reactive enough, surface accessible, and not a critical part of a protein's recognition regions. Cysteins and lysines are useful in this context because they have reactive functional groups and are typically exposed. An additional consideration is the number of sites, which should not exceed the desired protein:drug ratio, leading to heterogeneous products [Jung and Theato, 2013; An, 2009].

The most common strategies to generate protein-drug bioconjugates or to covalently link proteins to one another include the direct coupling using crosslinkers, or indirect coupling using activated functional groups. Crosslinkers are molecules that have readily reactive moieties at both ends. Homobifunctional (bearing the same reactive functional groups at both ends) and heterobifunctional crosslinkers (bearing different reactive functional groups at each end) are commercially available. The most common

crosslinkers are reactive towards primary amines or carboxylic acids, which are common moieties available at the proteins surface [Wong, 2011]. The indirect strategy of chemical coupling consists of activating a functional group, making it reactive towards a particular moiety, and then exposing it to that moiety. This coupling strategy is particularly useful when one of the two molecules to be conjugated have many functional groups available, making direct-crosslinking result in a mixture of conjugates. The most common indirect coupling strategies include the use of carbodiimide, maleimide, and activated esters functional groups [Mattson, 1993].

The ability to chemically modify proteins to produce bioconjugates with therapeutic applications is a valuable tool in the development of novel, protein based therapeutics. However, it is important to ensure that such modifications do not adversely affect the protein structure and function. In this dissertation, a DDS design is tested for protein function and structure integrity retention.

1.8 Photodynamic therapy

Photodynamic therapy (PDT) is an emerging cancer treatment that uses a type of drug called photosensitizer (PS). It has dual selectivity: after the PS accumulates in a target area, irradiation of visible light is applied in the presence of oxygen. Upon irradiation, the PS generates reactive oxygen species (ROS), causing oxidative damage and ultimately, cell death. The resulting damage is localized, given the reactive nature of the ROS.

Upon excitation (*hv*) of the PS, intersystem crossing may occur, resulting in two possible mechanisms for the generation of ROS. Type I reactions involve the formation of

radical intermediates that transfer their energy to oxygen to form superoxide anion radical (O_2^-) and hydroxyl radical ($OH^{\cdot}$). Type II reactions consist on the transfer of energy from the PS in the excited state to the triplet ground state of molecular oxygen ($^3O_2$) to produce singlet oxygen ($^1O_2$). Because the lifetime of the triplet excited state is longer than that of the singlet one, the type II mechanism typically predominates [De Rosa et al., 2002]. Even though tumor destruction by PDT is complex, including apostosis and necrosis, as well as induction of immunological responses and destruction of the tumor vasculature, $^1O_2$ is considered the main cytotoxic agent [Gomer et al., 2010; Nowis et al., 2005].

PS, which may be of natural or synthetic source, include a variety of molecules, such as tetrapyrroles, porphyrins, phtalocyanines, all of which can and have been functionalized with a wide variety of functional groups while retaining their phototoxicity. The earliest PS to be used and approved by the FDA for cancerous lesions is Photofrin®, an hematoporphyrin derivative that is comprised of a mixture of different molecules. This initial drug is known as the first generation PS. Second generation PS consist of pure and distinct molecules, many of which are modified in order to introduce desirable characteristics, such as absorption maxima at longer wavelengths, closer to the IR frequencies. Longest wavelength/lower energy radiation is preferred because it penetrates deeper into the tissue. Third generation PS are conjugated to delivery systems that increase selectivity for tumor tissues over healthy tissues, leading to some promising

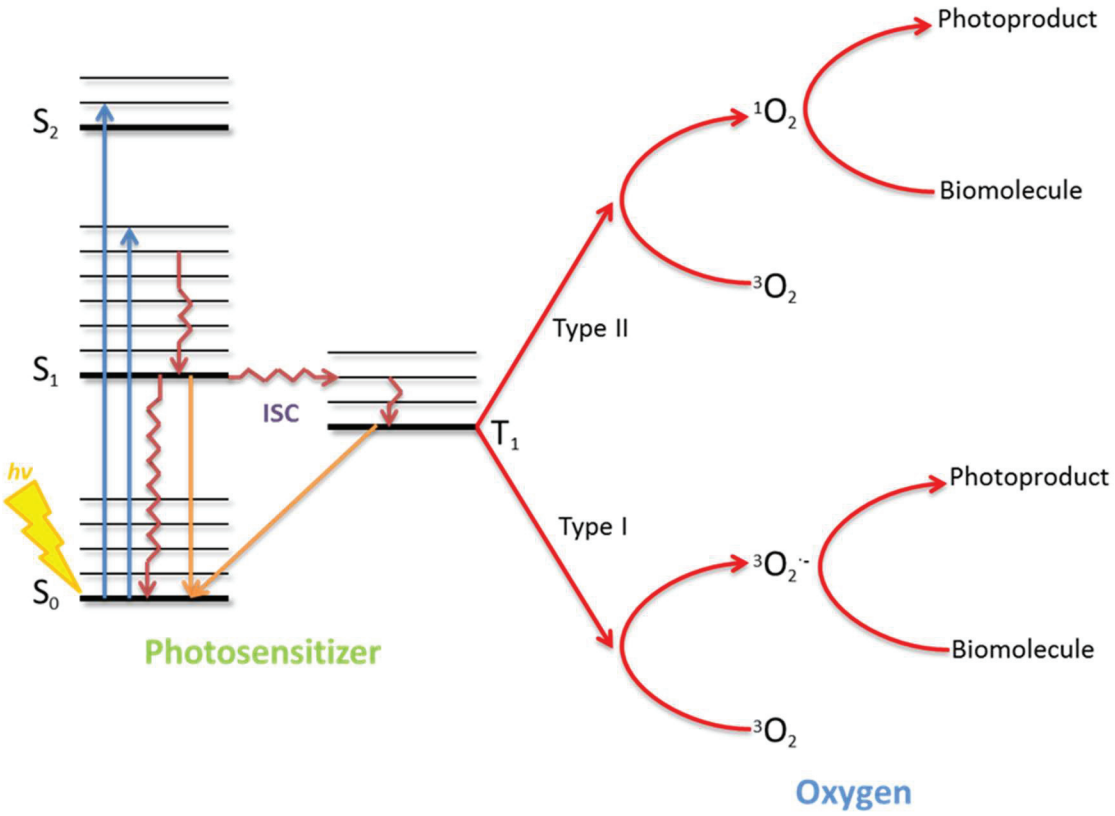

Figure 1.3 Scheme showing the two possible mechanisms for the generation of ROS by photosensitizers after irradiation. Type I reactions involve the formation of radical intermediates that transfer their energy to oxygen to form superoxide anion radical ($O_2^{\cdot-}$) and hydroxyl radical ($OH^{\cdot}$). Type II reactions consist on the transfer of energy from the PS in the excited state to the triplet ground state of molecular oxygen ($^3O_2$) to produce singlet oxygen ($^1O_2$). The type II mechanism typically predominates [De Rosa et al., 2002].

results [De Rosa et al., 2002; Josefsen et al., 2008]. The drawbacks of most photosensitizers include inappropriate tissue retention and activation energies, dark toxicity, hydrophobicity and lack of specificity; the non-selective accumulation of the PS can result in persistent skin photosensitivity [Allison et al., 2008]. The selectivity of the drug towards cancer tissue can be greatly enhanced by its coupling with an effective drug delivery system, and many efforts have been recently made in that direction.

Several types of PS have been coupled with HSA nanoparticles, resulting in enhanced delivery and cancer cell death both *in vitro* and *in vivo* [Chen et al., 2009; Jeong et al., 2011; Wacker et al., 2010]. PS have been conjugated to antibodies, sugars, oligonucleotides, aptamers, hormones, metabolites, cellular signaling species, peptides and proteins [Giuntini et al., 2011]. However, the coupling of the PS to nanoparticles generally results in quenching, hence inhibiting the generation of singlet oxygen. This quenching is reversible, as previous studies have shown, resulting in activation of the PS upon disintegration of the nanoparticles [Zeisser-Labouèbe et al., 2009]. This strategy enhances local activation of the drug, imparting the system with enhanced therapeutic index of photosensitizer and reduced photosensitivity in non-target organs.

In this work, the photosensitizer drug Chlorin e6 (Ce6) is used as a model for drug activation in dissolvable protein nanoparticles. Ce6 was selected because it is a well-known PS that is activated by near infrared wavelengths and has carboxylic groups available for modifications [Park and Na, 2013].

1.9 Nanoparticles for combination therapies

The most used treatment modalities for cancer include two or more therapeutic agents administered simultaneously. They may attack different targets, act synergistically, or lessen the side effects of other drugs. Combining different therapeutic agents into a single nano-platform can help regulate and enhance co-delivery. These delivery systems for combination therapy also serves to combine therapeutic and diagnostic tools in a single particle [Glasgow and Chougule, 2015; He et al., 2016].

Personalized medicine relies on the identification of "weak spots" in tumor cells genes to target them with specificity. As tumor biology knowledge and genomic testing tools continue to progress, personalized medicine will be increasingly the norm in cancer treatment. The design of robust models for drug delivery for combination therapy is essential in the advance of personalized medicine for cancer treatment. This dissertation focuses in the development of models for new protein-based nano-therapeutics with a focus on stimulus-responsive delivery and therapeutic protein function preservation.

1.10 Specific Aims

The following specific aims were designed to test the viability of redox-sensitive protein-based nanoparticles as therapeutic agents for cancer treatment:

Specific Aim #1: Redox responsive albumin nanoparticles for the intracellular delivery and activation of photosensitizers

Albumin nanoparticles were prepared by the desolvation technique and stabilized by a crosslinker with a disulfide bond in its spacer arm. This allows for protein dissolution into individual protein units when exposed to a reducing environment such as the cell

cytoplasm. A model photosensitizer, Ce6, was immobilized on the albumin nanoparticle surface. We hypothesized that the Ce6 immobilization on the nanoparticle would prevent phototoxicity due to photoquenching, and that the dissolution of the nanoparticle would result in drug activation only intracellularly. This model was successfully tested by proof-of-concept and *in vitro* experiments. Results showed that the introduction of redox sensitivity contributed to higher therapeutic photodynamic efficiency at lower doses after longer incubation times.

Specific Aim #2: To synthesize a redox responsive pro apoptotic protein-photosensitizer nanoparticle for cancer combination therapy

The pro apoptotic protein Cyt c was formulated into redox sensitive nanoparticles using the desolvation technique followed by crosslinking with DSP. Furthermore, the Cyt c nanoparticle surface was modified with Ce6 for co-delivery of the protein and the drug. Using the concepts proven in Specific Aim #1, the delivery system designed results in the selective intracellular activation of Ce6 as the cytochrome c is delivered to the cell cytoplasm. The cytotoxicity mechanisms of this delivery system and the effects of the covalent modification of the protein in its function and its pro apoptotic activity were evaluated. Also, the combination of the photosensitizer with the Cyt c was evaluated as a potential combination therapy for cancer. Previous studies have suggested that low-dose PDT can induce apoptosis instead of necrosis. For the first time, the pro apoptotic protein Cyt c is combined with low-dose Ce6 PDT to test its efficacy at inducing apoptosis.

1.11 Bibliography

Ahmed, A. A.; Etemadmoghadam, D.; Temple, J.; Lynch, A. G.; Riad, M.; Sharma, R.; Stewart, C.; Fereday, S.; Caldas, C.; Defazio, A.; Bowtell, D.; Brenton, J. D. Driver mutations in TP53 are ubiquitous in high grade serous carcinoma of the ovary. *J. Pathol*. **2010**, *221*, 49-56.

Alberts, B.; Johnson, A.; Lewis, J.; Raff, M.; Roberts, K.; Walter, P. Chapter 3: Proteins: Protein function. In *Molecular Biology of the Cell*, 6th ed.; Garland Science: New York, 2014; p 134-169.

Allison, R. R.; Mota, H. C.; Bagnato, V. S.; Sibata, C. H. Bio-nanotechnology and photodynamic therapy-State of the art review. *Photodiagn. Photodyn. Ther*. **2008**, *5*, 19-28.

Aylon, Y.; Oren, M. New plays in the p53 theater. *Curr. Opin. Genet. Dev*. **2011**, *21*, 86-92.

Carter, P. J. Introduction to current and future protein therapeutics: A protein engineering perspective. *Exp. Cell Res*. **2011**, *317*, 1261–1269.

Chen, K.; Preuβ, A.; Hackbarth, S.; Wacker, M.; Langer, K.; Röder, B. Novel photosensitizer-protein nanoparticles for photodynamic therapy: photophysical characterization and in vivo investigations. *Photochem. Photobiol. B*. **2009**, *96*, 66-74.

Choi, K. Y.; Swierczewska, M.; Lee, S.; Chen, X. Protease-activated drug development. *Theranostics,* **2012**, *2*, 156-178.

Danhier, F.; Feron, O.; Préat, V. To exploit the tumor microenvironment: Passive and active tumor targeting of nanocarriers for anti-cancer drug delivery. *J. Control. Release*. **2010**, *148*, 135-146.

DeRosa, M. C.; Crutchley, R. J. Photosensitized singlet oxygen and its application. *Coord. Chem. Rev*. **2002**, *233-234*, 351-371.

Desai, N. Nanoparticle albumin bound (nab) technology: targeting tumors through the endothelial gp60 receptor and SPARC. *Nanomedicine*. **2007**, *3*, 339.

Dinndorf, P. A.; Gootenberg, J.; Cohen, M. H.; Keegan, P.; Pazdur, R. FDA drug approval summary: pegaspargase (oncaspar) for the first-line treatment of children with acute lymphoblastic leukemia. *Oncologist*. **2007**, *12*, 991–998.

Dimitrov, D. S. Therapeutic proteins. *Methods Mol. Biol*. **2012**, *899*, 1-26.

Duggan, S. T.; Keating, G. M. Pegylated liposomal doxorubicin: a review of its use in metastatic breast cancer, ovarian cancer, multiple myeloma and AIDS-related Kaposi's sarcoma. *Drugs*. **2011**, 71, 2531-58.

Elbayoumi, T. A.; Torchilin, V. P. Tumor-specific antibody-mediated targeted delivery of Doxil reduces the manifestation of auricular erythema side effect in mice. *Int. J. Pharm*. **2008**, *357*, 272–279.

Elmore, S. Apoptosis: a review of programmed cell death. *Toxicol. Pathol*. **2007**, *35*, 495–516.

Fang, J.; Nakamura, H.; Maeda, H. The EPR effect: Unique features of tumor blood vessels for drug delivery, factors involved, and limitations and augmentation of the effect. *Adv. Drug Deliver. Rev*. **2011**, *63*, 136-151.

Gallo, J. M.; Hung, C. T.; Perrier, D. G. Analysis of albumin microsphere preparation. *Int. J. Pharm.* **1984**, *22*, 63-74.

Gillick, K.; Crompton, M. Evaluating cytochrome c diffusion in the intermembrane spaces of mitochondria durinig cytochrome c release. *J. Cell Sci*. **2008**, *121*, 618-626.

Giuntini, F.; Alonso, C. M. A.; Boyle, R. W. Synthetic approaches for the conjugation of porphyrins and related macrocycles to peptides and proteins. *Photochem. Photobiol. Sci.* **2011**, *10*, 759-791.

Glasgow, M. D. K.; Chougule, M. B. Recent developments in active tumor targeted multifunctional nanoparticles for combination chemotherapy in cancer treatment and imaging. *J. Biomed. Nanotechnol*. **2015**, *11*, 1859–1898.

Greish, K. Enhanced permeability and retention (EPR) effect for anticancer nanomedicine drug targeting. *Methods Mol. Biol*. **2010**, *624*, 25-37.

Gomer, C. J. *Photodynamic Therapy Methods in Molecular Biology*. Humana Press: New York, 2010.

Hanahan, D.; Weinberg, R. A. Hallmarks of cancer: the next generation. *Cell*. **2011**, *144*, 646-674.

He, C.; Tang, Z.; Tian, H.; Chen, X. Co-delivery of chemotherapeutics and proteins for synergistic therapy. *Adv. Drug Deliver. Reviews*. **2016**, *98*, 64-76.

Hong, R.; Han, G.; Fernández, J. M.; Kim, B. J.; Forbes, N. S; Rotello, V. M. Glutathione-mediated delivery and release using monolayer protected nanoparticle carriers. *J. Am. Chem. Soc*. **2006**, *128*, 1078-1079.

Housman, G.; Byler, S.; Heerboth, S.; Lapinska, K.; Longacre, M.; Snyder, N.; Sarkar, S. Drug resistance in cancer: an overview. *Cancers*. **2014**, *6*, 1769-1792.

Jaracz, S.; Chen, J.; Kuznetsova, L. V.; Ojima, I. Recent advances in tumor-targeting anticancer drug conjugates. *Bioorg. Med. Chem*. **2005**, *13*, 5043-5054.

Jeong, H.; Huh, M.; Lee, S. J.; Koo, H.; Kwon, I. C.; Jeong, S. Y.; Kim, K. Photosensitizer-conjugated human serum albumin nanoparticles for effective photodynamic therapy. *Theranostics*. **2011**, *1*, 230-239.

Josefsen, L. B.; Boyle, R. W. Photodynamic Therapy: Novel third-generation photosensitizers one step closer? *Br. J. Pharmacol*. **2008**, *154*, 1-3.

Kano, M. R.; Bae, Y.; Iwata, C.; Morishita, Y.; Yashiro, M.; Oka, M.; Fujii, T.; Komuro, A.; Kiyono, K.; Kaminishi, M.; Hirakawa, K.; Ouchi, Y.; Nishiyama, N.; Kataoka, K.; Miyazono, K. Improvement of cancer-targeting therapy, using nanocarriers for intractable solid tumors by inhibition of TGF-beta signaling. *PNAS*. **2007**, *104*, 3460–3465.

Karanth, H.; Murthy, R. S. pH-sensitive liposomes-principle and application in cancer therapy. *J. Pharm. Pharmacol*. **2007**, *59*, 469-483.

Kobayashi, H.; Brechbiel, M. W. Nano-sized MRI contrast agents with dendrimer cores. *Adv. Drug Deliver. Rev*. **2005**, *57*, 2271–2286.

Kobayashi, H.; Turkbey, B.; Watanabe, R.; Choyke, P. L. Cancer drug delivery: considerations in the rational design of nanosized bioconjugates. *Bioconjug. Chem*. **2014**, *25*, 2093–2100.

Kratz, F. Albumin as a drug carrier: design of prodrugs, drug conjugates and nanoparticles. *J. Control. Rel*. **2008**, *132*, 171-183.

Langer, K.; Balthasar, S.; Vogel, V.; Dinauer, N.; von Briesen, H.; Schubert, D. Optimization of the preparation process for human serum albumin (HSA) nanoparticles. *Int. J. Pharm*. **2003**, *257*, 169-180.

Leader, B.; Baca, Q. J.; Golan, D. E. Protein therapeutics: a summary and pharmacological classification. *Nat. Rev. Drug. Discov*. **2008**, *7*, 21-39.

Lee, K. S.; Chung, H. C.; Im S.A.; Park, Y. H.; Kim, C. S.; Kim, S. B.; Rha, S. Y.; Lee, M. Y.; Ro, J. Multicenter phase II trial of Genexol-PM, a Cremophor-free, polymeric micelle formulation of paclitaxel, in patients with metastatic breast cancer. *Breast Cancer Res. Treat*. **2008**, *108*, 241-50.

Lin, W.; Coombes, A. G. A.; Davies, M. C.; Davis, S. S.; Illum, L. Preparation of sub-100 nm human serum albumin nanospheres using a pH-coacervation method. *J. Drug Target*. **1993**, *1*, 237-243.

Liu, Y.; Wang, W.; Yang, J.; Zhou, C.; Sun, J. pH-sensitive polymeric micelles triggered drug release for extracellular and intracellular drug targeting delivery. *Asian J. Pharm. Sci*. **2013**, *8*, 159-167.

Lushchak, V. I. Glutathione Homeostasis and Functions: Potential Targets for Medical Interventions. *J. Amino Acids*. **2012**, *736837*, 1-26.

Maeda, H. Macromolecular therapeutics in cancer treatment: the EPR effect and beyond. *J. Control. Release*. **2012**, *164*, 138-144.

Mattson, G.; Conklin, E.; Desai, S.; Nielander, G.; Savage, M. D.; Morgensen S. A practical approach to crosslinking. Special Issue: Protein-Protein Interactions. *Mol. Biol. Rep*. **1993**, *17*, 167-183.

Mendez, J.; Monteagudo, A.; Griebenow, K. Stimulus-responsive controlled release system by covalent immobilization of an enzyme into mesoporous silica nanoparticles. *Bioconj. Chem*. **2012**, *23*, 698-704.

Miele, E.; Spinelli, G. P.; Miele, E.; Tomao, F.; Tomao, S. Albumin-bound formulation of paclitaxel (Abraxane® ABI-007) in the treatment of breast cancer. *Int. J. Nanomed*. **2009**, *4*, 99–105.

Müller, B. G.; Leuenberger, H.; Kissel, T. Albumin nanospheres as carriers for passive drug targeting: an optimized manufacturing technique. *Pharm. Res*. **1996**, *13*, 32-37.

Narang, A. S.; Varia, S. Role of tumor vascular architecture in drug delivery. *Adv. Drug Deliver. Rev*. **2011**, *63*, 640-658.

Nowis, D.; Makowski, M.; Stoklosa, T.; Legat, M.; Issat, T.; Golab, J. Direct tumor damage mechanisms of photodynamic therapy. *Acta Biochim. Pol.* **2005**, *52*, 339-352.

Park, H.; Na, K. Conjugation of the photosensitizer Chlorin e6 to pluronic F127 for enhanced cellular internalization for photodynamic therapy. *Biomaterials*. **2013**, *34*, 6992–7000.

Petre, C. E.; Dittmer, D.P. Liposomal daunorubicin as treatment for Kaposi's sarcoma. *Int. J. Nanomed*. **2007**, *2*, 277–288.

Pillai, G. Nanomedicines for cancer therapy: an update of FDA approved and those under various stages development. *SOJ Pharm. Pharm. Sci*. **2014**, *1*, 13.

Riggio, C.; Pagni, E.; Raffa, V.; Cuschieri, A. Nano-oncology: clinical application for cancer therapy and future perspectives. *J. Nanomater*. **2011**, *164506*, 1-10.

Rivlin, N.; Brosh, R.; Oren, M.; Rotter, V. Mutations in the p53 tumor suppressor gene: important milestones at the various steps of tumorigenesis. *Genes Cancer*. **2011**, *2*, 466–474.

Rosano, G. L.; Ceccarelli, E. A. Recombinant protein expression in *Escherichia coli*: advances and challenges. *Front. Microbiol*. **2014**, *5*, 172.

Schroeder, A.; Heller, D. A.; Winslow, M. M.; Dahlman, J. E.; Pratt, G.W.; Langer, R.; Jacks, T.; Anderson. D. G. Treating metastatic cancer with nanotechnology. *Nat. Rev. Cancer*. **2011**, *12*, 39-50.

Sun, T.; Zhang, Y. S.; Pang, B.; Hyun, D. C.; Yang, M.; Xia, Y. Engineered nanoparticles for drug delivery in cancer therapy. *Angew. Chem. Int. Ed*. **2014**, *53*, 12320–12364.

Torchilin, V. Tumor delivery of macromolecular drugs based on the EPR effect. *Adv. Drug Deliv. Rev*. **2011**, *63*, 131-135.

Torchilin, V. P. Multifunctional, stimuli-sensitive nanoparticulate systems for drug delivery. *Nat. Rev. Drug Discov*. **2014**, *13*, 813-827.

Yousefpour, P.; Chilkoti, A. Co-opting biology to deliver drugs. *Biotechnol. Bioeng*. **2014**, *111*, 1699–1716.

Raj, T. A.; Smith, A. M.; Moore, A. S. Vincristine sulfate liposomal injection for acute lymphoblastic leukemia. *Int. J. Nanomed*. **2013**, *8*, 4361-4369.

Vhora, I.; Patil, S.; Bhatt, P.; Misra, A. Chapter 1: Protein- and peptide-drug conjugates: an emerging drug delivery technology. In *Advances in Protein Chemistry and Structural Biology*; Donev, R., Ed.; Elsevier Science: Amsterdam, 2015, Vol 98; p. 1-55.

Wacker, M.; Chen, K.; Preuss, A.; Possemeyer, K.; Röder, B.; Langer, K. Photosensitizer loaded HSA nanoparticles. I: Preparation and photophysical properties. *Int. J. Pharm*. **2010**, *393*, 253-262.

Wang, W.; Wang, E. Q.; Balthasar, J.P. Monoclonal antibody pharmacokinetic and pharmacodynamics. *Clin. Pharmacol. Ther*. **2008**, *84*, 548-558.

Wong, S. S.; Jameson, D. M. *Chemistry of Protein and Nucleic Acid Cross-Linking and Conjugation*, 2nd ed.; CRC Press: Boca Raton, 2011.

Zahid, M.; Robbins, P. D. Cell-type specific penetrating peptides: Therapeutic promises and challenges. *Molecules*. **2015**, *20*, 13055-13070.

Zeisser-Labouèbe, M.; Mattiuzzo, M.; Lange, N.; Gurny, R.; Delie, F. Quenching-induced deactivation of photosensitizer by nanoencapsulation to improve phototherapy of cancer. *J. Drug Targ*. **2009**, *17*(8), 619-626.

Zhao, M.; Biswas, A.; Hu, B.; Joo, K.I.; Wang, P.; Gu, Z.; Tang, Y. Redox-responsive nanocapsules for intracellular protein delivery. *Biomaterials*. **2011**, *32*, 5223-5230.

Zhou, M.; Li, Y.; Hu, Q, Bai, X.; Huang, W.; Yan, C.; Scheres, S. H. W.; Shi, Y. Atomic structure of the apoptosome: mechanism of cytochrome c- and dATP-mediated activation of Apaf-1. *Genes Dev*. **2015**, *29*, 2349-2361.

Chapter 2

Materials and methods

2.1 Experimental procedures – Chapter 3

2.1.1 Materials

Chlorin e6 (Ce6) was purchased from Frontier Scientific, Logan, UT. HSA, ethanol (≥99.5%), DMSO (≥99.9%), glutaraldehyde (25% in water), 1-ethyl-3-[3-dimethylaminopropyl]carbodiimide hydrochloride (EDC), N-hydroxysuccinimide (NHS), and reduced glutathione ethyl ester were obtained from Sigma-Aldrich (St. Louis, MO). Dithiobis[succinimidyl propionate] (DSP) was purchased from Thermo, Waltham, MA. 4', 6-Diamidino-2-phenylindole (DAPI), propidium iodide (PI), and FM-4-64 membrane stain were purchased from Invitrogen (Grand Island, NY). All reagents were used without further purification. HeLa, A549, and HUVEC cells were purchased from the American Type Culture Collection (Manassas, VA).

2.1.2 Preparation of the HSA-Ce6-FA nanoparticles

2.1.2.1 Synthesis of the NHS ester of Ce6. The Ce6 NHS-ester was synthesized by reacting 2.5 equivalents of EDC and 5 equivalents of NHS with 1 equivalent of Ce6 in a solution of 2:1 ethanol:MES buffer (vol:vol) at a pH of 6.0. The product of this reaction was precipitated by the addition of MES buffer followed by centrifugation for the removal of excess EDC and NHS.

2.1.2.2 Preparation and crosslinking of the HSA nanoparticles. The HSA nanoparticles were prepared by a modified method according to Langer et al. [2003]. Briefly, HSA was dissolved in 10 mM NaCl, pH 9.0, to achieve a final concentration of 25 mg/ml. Ethanol was added at a constant rate of 1 ml/min with an automated syringe to reach a final ratio of 1:4 water:ethanol under stirring. Immediately afterwards, either dithiobis[succinimidyl propionate] (DSP) in DMSO or glutaraldehyde (25%) in water was added to achieve nanoparticle crosslinking. Since the nanoparticles consist of a water-soluble protein the crosslinking was essential to prevent dissolution of the nanoparticles upon exposure to an aqueous environment (e.g. reconstitution buffer, blood).

2.1.2.3 Surface modification of HSA nanoparticles with Ce6. The purified Ce6 NHS-ester was dissolved in pure ethanol and its concentration was determined from its absorbance at 400 nm using the extinction coefficient of 211.16 ml/(mg·cm). The reaction product was then added to the nanoparticle suspension at an excess and was left to react overnight. The modified nanoparticles were centrifuged at 11000 rpm, resuspended in water, and the supernatant was discarded. This washing step was repeated twice to remove the drug that was not covalently attached. The drug loading was determined by measuring the UV/Vis absorption at 400 nm of the supernatants discarded and subtracting it from the initial Ce6 NHS-ester concentration.

2.1.3 Particle size, polydisperity, and zeta potential measurements

Size, polydispersity, and zeta potential of the Ce6-HSA nanoparticles were determined by dynamic light scattering (DLS) using a Malvern Zetasizer Nanoseries. The samples were dispersed in nanopure water and sonicated until a good suspension was obtained. The protein mode was selected and the Average-Z was used. All of the measured nanoparticle suspensions showed only one peak.

2.1.4 Scanning electron microscopy of HSA-Ce6 nanoparticles

The morphology was examined by a JEOL 5800 LV scanning electron microscopy (SEM) at 20 kV. The samples were coated with gold for 10 seconds in a Denton Vacuum DV- 502A.

2.1.5 Degree of nanoparticle crosslinking

The average number of amines of the HSA modified by DSP was determined by the 2,4,6-trinitrobenzene sulfonic acid (TNBSA) chromogenic assay after disintegration of the nanoparticle with a DTT solution [Habeeb, 1966]. The TNBSA reacts with the unmodified primary amines to produce absorbance at 335 nm. Briefly, the crosslinked nanoparticles were suspended in a solution containing 20 mM DTT, and were kept stirring for 2 h. The treated protein was filtered using a centrifugal filter unit (Millipore) to remove the DTT. The soluble protein was dissolved in 0.1 M sodium bicarbonate, pH 8.5 and adjusted to a concentration of 0.095 mg/ml by measuring its absorbance at 280 nm against a calibration curve. This concentration was determined by optimization of this

method for albumin. 250 µL de 0.01% TNBSA were added to 500 µL of each solution. All the solutions were incubated at 37°C for 2 hours. Then, 250 µL of 10 % SDS y 125 µL of 1M HCl were added to stop the reaction. The absorbance of each solution was measured at 335 nm. The amount of lysines modified by the crosslinker was determined against a calibration curve of native albumin (0.025-0.2 mg/ml) reacted with TNBSA. All samples were analyzed in triplicate.

2.1.6 Nanoparticle disintegration and fluorescence

The disintegration of the nanoparticles was evaluated by a turbidity assay. Briefly, the glutaraldehyde crosslinked Ce6-HSA nanoparticles and the DSP-crosslinked Ce6-HSA nanoparticles were incubated in a 10 mM glutathione solution. Aliquots of each suspension were retrieved at predetermined times and the absorbance at 700 nm was measured. It has to be noted that the absorbance of Ce6 is negligible at 700 nm while significant at shorter wavelengths. The absorption was plotted against time and normalized to 100% turbidity at t=0. To evaluate the changes in fluorescence intensity, the nanoparticles were suspended in a reducing media (10 mM GHS in PBS) and the fluorescence spectra were obtained at predetermined times using a Varian Cary Eclipse Fluorescence Spectrophotometer. A nanoparticle suspension in non-reducing PBS was used as control.

2.1.7 Singlet oxygen generation

The generation of singlet oxygen by DSP-crosslinked Ce6-HSA nanoparticles, glutaraldehyde-crosslinked Ce6- HSA nanoparticles, and free Ce6 was determined by the

p-nitrosodimethylaniline (RNO) bleaching method [Kraljic and El-Mohsni, 1978; Bose and Dubue, 2008; Meerovich et al., 2014]. Singlet oxygen reacts with imidazole to form intermediate products that proportionally oxidize RNO, bleaching its absorbance at 440 nm. Briefly, the Ce6-HSA nanoparticles crosslinked with either DSP or glutaraldehyde were suspended in phosphate buffer (pH=7.4) in reducing (10 mM glutathione) or non-reducing conditions. The suspensions were mixed with imidazole (10 μM) and RNO (50 μM). Immediately afterwards, they were irradiated with a LED lamp (λmax=660 ± 10 nm) at a fixed distance of 5 cm and a fluence rate of 50 mW/cm^2, while bubbling with oxygen. Aliquots were retrieved every five minutes, centrifuged (11,000 rpm, 1 minute), and the supernatant absorbance was measured at 440 nm. The results were normalized to abs=0 at t=0.

2.1.8 Mammalian cell culture

HeLa cells (human epithelial cervix adenocarcinoma), A549 cells (human lung carcinoma), and HUVEC cells (human endothelial umbilical vein normal cells) were cultured according to the instructions given by the American Type Culture Collection. The cells were grown in minimum essential medium (MEM) or Ham's F-12 medium containing 1% L-glutamine, 10% fetal bovine serum (FBS), and 1% penicillin in a humidified incubator with 5% CO_2 and 95% air at 37°C. All experiments were conducted before the cells reached 20 passages.

2.1.9 Cell viability assay

HeLa, A549, or HUVEC cells were seeded in 96-well plates for 24 h in MEM or Ham F-12 containing 1% L-glutamine, 10% FBS, and 1% penicillin. The cell growth was then arrested by decreasing the FBS concentration in the medium to 1% for 18 h. Subsequently, the cells were washed with PBS, and incubated with the glutaraldehyde or DSP-crosslinked Ce6-HSA nanoparticles at varying concentrations (5-50 ng/ml) and incubation times (1, 6, or 24 h). For photo toxicity experiments, the cells were irradiated with a LED lamp (λmax=660 ± 10 nm) placed at a distance of 8 cm from the cell plate immediately after incubation for a total light dose of 3 J/cm^2. For cell viability measurements, the CellTiter 96 aqueous nonradioactive cell proliferation assay (Promega, Madison, WI) was used. 20 µL of 3-(4,5-dimethylthiazol-2-yl)-5-(3 carboxymethoxyphenyl)-2-(4-sulfophenyl)-2H-tetrazolium, inner salt (MTS) and phenazine methosulfate (PMS) was added to each well (333 µg/mL MTS and 25 µM PMS) and after 1 hour the absorbance at 492 nm was measured using a microplate reader. Untreated cells were used as a negative control.

2.1.10 Caspase activation assay

HeLa cells were grown to 80% confluency, harvested, washed, and finally disrupted. For disruption the cells were suspended in a homogenizing buffer containing 20 mM 4-(2-hydroxyethyl)-1-piperazineethanesulfonic acid (HEPES) at pH 7.5, 10 mM KCl, 1.5 mM $MgCl_2$, 1 mM sodium EDTA, 1 mM sodium EGTA, 1 mM DTT, 250 mM sucrose, and a cocktail of serine, cysteine, aspartic acid, and metalloprotease inhibitors (1X). The

suspended cells were frozen in liquid N_2 for 2 minutes and thawed in a 37°C water bath and the freeze/thaw cycle repeated three times. The protein content in the lysate was determined using the Bradford assay. The cell-free reactions were performed in homogenizing buffer in a total volume of 100 µL. The cell-free reaction was initiated by adding the free Ce6 and each HSA-Ce6 nanoparticle suspension to freshly purified lysate adjusted to a total protein concentration of 3mg/ml in a total reaction volume of 100µL. The reaction was incubated at 37°C for 150 min. Afterwards, the caspase-3 assay was performed following the manufacturer's protocol (CaspACE™ assay; Promega, Madison, WI). Briefly, 20 µL of the reaction mixtures were withdrawn and added to 78 µL of a mixture containing 100 mM HEPES (pH 7.5), 10% w/v sucrose, 0.1% w/v CHAPS (3-[(3-cholamido-propyl)-dimethylammonio]-1-propane-sulfonate), 10 mM DTT, and 2% v/v DMSO. Afterwards, 2 µL of 10 mM DEVD-pNA substrate was added to each sample. The plate was incubated overnight at room temperature and the absorbance at 405 nm was measured in each well using a microplate reader (Thermo Scientific Multiskan FC). All measurements were performed in triplicate.

2.1.11 Confocal microscopy-cell death induction

HeLa cells were seeded as described before in lab-tek chambered coverslides (4 wells) for their examination by confocal laser scanning microscopy. The cells were incubated with the glutaraldehyde or the DSP-crosslinked Ce6-HSA nanoparticles at a Ce6 concentration of 10 ng/ml for 6 hours and irradiated for 10 minutes exactly as described above for a total light dose of 1.5 J/cm^2. The cells were washed with PBS (2x, 3 minutes)

and incubated with DAPI (300 nM) and next with PI (75 µM) for 5 minutes each. A solution of 3.7% formaldehyde was used to fix the cells. The HeLa cells were examined under a Zeiss laser scanning microscope 510 using a 67× objective. DAPI was excited at 405 nm and its emission was detected at 420–480 nm. PI was excited at 561 nm and its emission was detected at 600–674 nm.

2.1.12 Confocal microscopy - endosomal escape

The internalization of the bioconjugates and their ability to escape endosomal entrapment were determined by confocal laser scanning microscopy. The glutaraldehyde and the DSP-crosslinked Ce6-HSA nanoparticles were labeled with FITC. The cells were incubated with FITC-labeled Ce6-HSA nanoparticles at a drug concentration of 10 ng/ml and an endosome marker (FM-4-64; 10 µg/mL) at 37°C for 24 hours in the dark. Then the medium was removed and the cells were washed with PBS three times, and fixed with 3.7% formaldehyde. The coverslips were examined as described before and excited at 488 nm. FITC fluorescence was detected at wavelengths between 513 and 588 nm and the endosome marker between 598 and 738 nm.

2.1.13 Statistical analysis

The relative cell viability (%) was calculated by the formula: relative cell viability (%)=(Abs test sample/Abs untreated cells) × 100. The results were expressed as mean ± SD. Mann Whitney analysis was used for comparison of two independent groups for cell viability in dark toxicity experiments using Stata® software. Difference between control (untreated cells) and experimental group (glutaraldehyde and DSP crosslinked

nanoparticles) was considered statistically significant at $p<0.05$. Two tailed t-test analysis was performed for comparison of two independent groups using SigmaPlot 12.0 software in time- and dose-dependent cell viability experiments. A p-value <0.05 was considered statistically significant within the 95% confidence interval. In all experiments, n=8.

2.2 Experimental procedures – Chapter 4

2.2.1 Materials

Chlorin e6 (Ce6) was purchased from Frontier Scientific, Logan, UT. Cytochrome c (Cyt c) from equine heart, ethanol (≥99.5%), DMSO (≥99.9%), 1-ethyl-3-[3-dimethylaminopropyl]carbodiimide hydrochloride (EDC), N-hydroxysuccinimide (NHS), and reduced glutathione ethyl ester were from Sigma-Aldrich (St. Louis, MO). Dithiobis[succinimidyl propionate] (DSP) was from Thermo (Waltham, MA). Acetonitrile (HPLC grade) was from Fisher (Waltham, MA). 4', 6-Diamidino-2-phenylindole (DAPI) and propidium iodide (PI) were purchased from Invitrogen (Grand Island, NY). All the reagents were used without further purification. All other chemicals were from various commercial suppliers and were at least of analytical grade. HeLa cells were purchased from the American Type Culture Collection (Manassas, VA) and grown according to the vendor's instruction.

2.2.2 Preparation of redox sensitive Cyt c nanoparticles

Briefly, Cyt c was solvent-precipitated from nanopure water by adding acetonitrile at a final 1:4 volume ratio at a constant rate of 120 ml/min using an automated syringe

[Morales-Cruz, 2015]. Different protein concentrations (5, 10, 25 mg/ml) were tested. After precipitation, DSP crosslinker was added and incubated for 30 minutes with continuous stirring. Different crosslinking ratios were tested and evaluated in terms of nanoparticle size and release profile. The nanoparticles were subsequently centrifuged at 10000 rpm, and washed twice with nanopure water. Then they were flash-frozen and freeze-dried.

2.2.3 Cyt c nanoparticle surface modification with Ce6 NHS ester

Ce6 NHS ester was prepared as described in the section 2.1.2.1. The dry crosslinked Cyt c nanoparticles were weight and suspended in PBS, pH 7.0. A known amount of Ce6 NHS ester was added to the nanoparticle suspension and the reaction proceeded overnight. Then, the nanoparticle suspension was purified to remove the drug that was not covalently attached using a centrifugal filter unit (3 kDa membrane, Millipore). The amount of drug immobilized in the nanoparticle was determined by subtracting the amount of drug released from the amount added to the reaction against a calibration curve.

2.2.4 Size measurements

Size and polydispersity of the Ce6-HSA nanoparticles were determined by dynamic light scattering (DLS) using a Malvern Zetasizer Nanoseries. The samples were dispersed in nanopure water and sonicated until a good suspension was obtained. The protein mode was selected and the Average-Z was used.

2.2.5 Protein release in reducing environment

The Cyt c nanoparticles were suspended in PBS EDTA containing 10 mM glutathione at a concentration of 1.5 mg/ml. They were incubated at 37°C while stirring with a magnetic bar. At each predetermined time, the suspension was centrifuged at 8000 rpm for 10 min, RT. The supernatant was removed and its absorption at 408 nm was measured. The amount of Cyt C dissolved was determined against a calibration curve of Cyt c in PBS EDTA at 408 nm. The pellet was then resuspended in freshly prepared buffer to continue incubation. Non-reducing PBS was used as control. All measurements were conducted in triplicate.

2.2.6 Gel Electrophoresis of released Cyt c

Cyt c nanoparticle dissolution was confirmed by reducing SDS polyacrylamide gel electrophoresis (PAGE). Briefly, the native Cyt c, the Cyt c nanoparticles, and the Cyt c-Ce6 nanoparticles (low drug ratio) were suspended at a concentration of 0.5 mg/ml in PBS, pH 7.0. The samples were diluted in sample buffer containing 10 % SDS and 10 mM 2-mercaptoethanol, and heated to 95°C for 5 minutes. The gel was run at 120 V and stained with Coomasie Brilliant Blue.

2.2.7 Cell culture

HeLa cells (human epithelial cervix adenocarcinoma) were cultured according to the instructions given by the American Type Culture Collection. The cells were grown in minimum essential medium (MEM) containing 1% L-glutamine, 10% fetal bovine serum

(FBS), and 1% penicillin in a humidified incubator with 5% CO2 and 95% air at 37°C. All experiments were conducted before the cells reached 20 passages.

2.2.8 Residual activity after system release-caspase activation

HeLa cells were seeded in black 96-well plates with clear bottoms for 24 h in 100 µL of MEM containing 1% L-glutamine, 10% FBS, and 1% penicillin. The cell growth was then arrested by removing the media and replacing it with MEM with 1% FBS for at least 18 h. Native Cyt c, Cyt c nanoparticles, free Ce6, and Cyt c-Ce6 nanoparticles were added to the cells for a final Cyt c concentration of 75 µg/ml. After incubation for 6 hours, the Apo-ONE® Homogeneous Caspase-3/7 Assay (Promega) was used and the manufacturer's protocol was followed. The Apo-ONE® Caspase-3/7 Reagent was added to the treated and control cells and mixed gently for 30 seconds. After 30 min, the fluorescence was measured, with an excitation wavelength of 499 nm and an emission wavelength of 521 nm using a Tecan Infinite® 200 PRO series. MEM and untreated cells were used as negative controls.

2.2.9 Circular Dichroism (CD) spectroscopy

The structural changes in Cyt c as a result of nanoparticle formulation and covalent immobilization of the Ce6 were studied by CD spectroscopy. The Cyt c and the Cyt c-Ce6 nanoparticles were suspended in reducing media (PBS, 0.1 mM, pH 7.0, with 10 mM glutathione) and incubated for 2 hours. The released Cyt c concentration was adjusted to approximately 0.09 mg/ml. CD spectra were obtained using a JASCO J-1500 High Performance CD spectrometer at room temperature. Far-UV spectra were measured from

190-250 nm to study the changes in secondary structure. Near-UV spectra were measured from 260-350 nm to observe the protein tertiary structure. Each sample was scanned thrice to obtain an averaged spectrum from which the background of PBS was subtracted. The native Cyt c adjusted to 0.09 mg/ml in PBS was used as control.

2.2.10 Cell viability

HeLa cells were seeded in 96-well plates for 24 h in MEM containing 1% L-glutamine, 10% FBS, and 1% penicillin. The cell growth was then arrested by decreasing the FBS concentration in the medium to 1% for 18 h. Subsequently, the cells were incubated with the native Cyt c, the Cyt c nanoparticles and Cyt c-Ce6 nanoparticles. For dose response experiments, the cells were incubated at varying Cyt c concentrations (10-100 µg/ml) for 6h. For photo toxicity experiments, the cells were irradiated with a LED lamp (λ_{max}=660 ± 10 nm) placed at a distance of 8 cm from the cell plate immediately after incubation for 5 minutes. For cell viability measurements, the CellTiter 96 aqueous nonradioactive cell proliferation assay (Promega, Madison, WI) was used. 20 µL of MTS and PMS was added to each well (333 µg/mL MTS and 25 µM PMS) and after 1 h the absorbance at 492 nm was measured using a microplate reader. Untreated cells were used as a negative control.

2.2.11 Confocal microscopy - cell internalization studies

HeLa cells were seeded in lab-tek chambered coverslides (4 wells) at a concentration of 2.5 x 10^6 cells/ml for their examination by confocal laser scanning microscopy. The native Cyt c, Cyt c nanoparticles and Cyt c-Ce6 nanoparticles were

labeled with fluorescein isothiocyanate (FITC, Sigma). The cells were incubated with FITC-labeled bioconjugates at a Cyt c concentration of 75 μg/ml at 37°C for 6 h in the dark. Then the medium was removed and the cells were washed with PBS three times, and fixed with 3.7% formaldehyde. The coverslips were examined as described before and excited at 488 nm. FITC fluorescence was detected at wavelengths between 513 and 588. Untreated cells were used as control and to detect auto fluorescence.

2.2.12 Confocal microscopy – Apoptosis induction

HeLa cells were seeded in lab-tek chambered coverslides (4 wells) at a concentration of 2.5 x 10^6 cells/ml and treated with Annexin V conjugated to FITC and PI (Life Technologies) to identify apoptotic from necrotic cells. Briefly, cells were incubated with native Cyt c, Cyt c nanoparticles, and Cyt c-Ce6 nanoparticles to a final Cyt c concentration of 75 μg/ml for 6 h. Subsequently, the cells were washed with PBS, incubated with Annexin V and PI, and fixed with 3.7% formaldehyde. The coverslides were examined by confocal laser scanning microscopy. Annexin V labeled with FITC was excited at 494 nm and its emission at 518 nm was measured. Propidium iodide was excited at 535 nm and its emission was detected at 617 nm. Untreated cells were used as a negative control and to detect cell auto fluorescence.

2.2.13 Membrane integrity assay

The membrane integrity disruption as a result of necrosis induction was evaluated. The release of lactate dehydrogenase, a stable cytosolic enzyme was measured with the CytoTox 96® Non-Radioactive Cytotoxicity Assay (Promega). Briefly, the HeLa cells were

seeded in 96-well plates. After cell-cycle arrest, the cells were incubated with native Cyt c, Cyt c nanoparticles, Ce6, and Cyt c-Ce6 nanoparticles. Protein concentration in all samples was adjusted to 75 µg/ml, and Ce6 concentration was 2 µg/ml. After 6 hours, the samples were irradiated for 5 minutes as described in section 2.2.10. In a separate plate, the same samples were kept in the dark as a control. Then, 100 µl of the supernatant were transferred to a new 96-well plate, onto which 100 µl of CytoTox 96® Reagent were added. After a 30-minute incubation at room temperature, a stop solution is added, and the absorbance signal is measured at 490nm in a microplate reader.

2.2.14 Statistical Analysis

Mann–Whitney analysis was used for comparison of two independent groups. The difference between control and experimental groups was considered statistically significant at $p<0.05$. For comparison of multiple groups, ANOVA analysis was used. All of the experiments were at least performed in triplicate, the results averaged, and the standard deviation (SD) or standard error of the mean (SEM) calculated.

2.3 Bibliography

Bose, B.; Dube, A. Photodynamic efficacy of chlorin p6: a pH dependent study in aqueous and lipid environment. *J. Photochem. Photobiol.* **2008**, 93, 32-35.

Habeeb, A. F. Determination of Free Amino Groups in Proteins by Trinitrobenzenesulfonic Acid. *Anal. Biochem*. **1966**, 14, 328–336.

Kraljic, I.; El-Mohsni. S. A new method for detection of singlet oxygen in aqueous solution. *Photochem. Photobiol.* **1978**, 28, 577-581.

Langer, K.; Balthasar, S.; Vogel, V.; Dinauer, N.; von Briesen, H.; Schubert, D. Optimization of the preparation process for human serum albumin (HSA) nanoparticles. *Int. J. Pharm*. **2003**, *257*, 169-180.

Meerovich, I.; Muthukrishnan, N.; Johnson, G.A.; Erazo-Oliveras, A.; Pellois, J.P. Photodamage of lipid bilayers by irradiation of a fluorescently labeled cell-penetrating peptide. *Biochim. Biophys. Acta.* **2014**, 1840, 507-515.

Morales-Cruz, M.; Figueroa, C.M.; González-Robles, T.; Delgado, Y.; Molina, A.; Méndez, J.; Morales, M.; Griebenow, K. Activation of caspase-dependent apoptosis by intracellular delivery of Cytochrome c-based nanoparticles. *J. Nanobiotechnol*. **2014**, *12*, 33.

Chapter 3

Redox-Sensitive Crosslinking Impact on Albumin Nanoparticle Function as Delivery System for Photodynamic Cancer Therapy

3.1 Summary

Photodynamic therapy (PDT) is a promising alternative to traditional chemotherapy, and has been increasingly the subject of research for the treatment of cancer. One of its advantages oven chemotherapeutic agents is that it does not result in systemic toxicity and the generation of multidrug resistance [Plichenkov et al., 2014; Allison et al., 2008]. It relies on the accumulation of photosensitizer drugs in a target area and the subsequent application of irradiation in the presence of oxygen. Upon irradiation, the photosensitizer generates reactive oxygen species (ROS), causing oxidative damage and localized cell death, given the reactive nature of the ROS [Allison, 2014].

Photosensitizers have been coupled with several delivery systems that effectively overcome some of the drugs limitations, such as tumor tissue selectivity and dark toxicity. These systems include liposomes, synthetic polymer-based micelles, and inorganic nanoparticles, among others [Shirasu, 2013]. PS have also been conjugated to peptides and proteins for passive as well as active targeting [Giuntini et al., 2011].

Human serum albumin (HSA) is the most abundant protein in human plasma with a long blood half-life, and plays a determinant role in the transport of many metabolic

compounds and drugs [Li et al., 2008]. Since it is generally non immunogenic, it is very attractive as a drug carrier. Moreover, it has been described to preferentially accumulate in tumor and inflamed tissue, a property being exploited in the FDA approved anti-cancer drug Abraxane® [Kratz, 2008]. Several PS drugs have been immobilized in HSA nanoparticles through adsorption [Chen et al., 2009, Wacker et al., 2010, Preuss et al., 2011]. A significant drawback of this type of binding is that the leaching of the drug from the carrier can occur during delivery and before effective accumulation in the target tissue takes place. A comparative study of PS-loaded and conjugated glycol chitosan nanoparticles found that covalently bound drug resulted in enhanced efficiency *in vivo* over physically loaded drug due to its prolonged circulation time and higher accumulation in the tumor site [Lee et al., 2011]. In this study we developed an albumin-based drug delivery system onto which the model PS drug is covalently attached.

The covalent immobilization of PS in delivery systems leads to photoquenching, inactivating the photodynamic activity. The photoquenching can be reversible if the system is designed to degrade at the target site, as a previous study shows [Zeisser-Labouèbe et al., 2009]. Degradable protein nanoparticles are being explored in this work as delivery systems for a model photosensitizer drug to target solid tumors. Herein we developed a drug delivery system involving stimulus-responsive (thiol-cleavable) crosslinking. The crosslinker forms stable bonds in solution under aerobic conditions preventing disintegration of the protein nanoparticles during delivery. However, when exposed to a reducing environment, such as the cell interior, the nanoparticles break down. This in turn should lead to reduced photoquenching of the PS drug and improve

the generation of singlet oxygen upon irradiation. The cytosol of cells is much more reducing than the extracellular space due to the presence of reducing agents, mainly glutathione, at a much higher concentration than at the extracellular space. Hence, a thiol cleavable crosslinker is an attractive candidate for intracellular drug activation. In this study we systematically compare the Ce6-HSA nanoparticles crosslinked with a thiol-cleavable crosslinker with particles prepared using glutaraldehyde, which leads to redox-insensitive crosslinking.

The model photosensitizer drug selected for this study was Chlorin e6 (Ce6), a second-generation photosensitizer activatable by near-infrared wavelengths. This drug was selected due to its high photodynamic efficiency as well as the available moieties for covalent coupling to the drug delivery system. The coupling of the photosensitizer to a nanoparticle or another macromolecule generally results in non-photochemical excitation quenching which drastically reduces the generation of singlet oxygen. Additionally, the system designed must fulfill specific size criteria to take advantage of passive targeting via the EPR effect. In general, nanoparticles from 100 to 800 nm can enter the irregular tumor fenestrae, but must be bigger than 20 nm to avoid renal filtration [Torchilin, 2011; Schroeder et al., 2011]. Herein, the synthesis of the HSA-Ce6 nanoparticles stabilized by either glutaraldehyde or the redox-sensitive crosslinker was optimized to obtain particles of appropriate size and shape, and its behavior in a reducing environment was evaluated. Furthermore, the delivery system behavior *in vitro*, namely the induction of dark toxicity, the dose and incubation time, as well as the internalization and intracellular fate was determined.

3.2 Results and Discussion

PDT ideally has dual selectivity: first, it can preferentially be accumulated in the target tissue, and second, oxidative damage is induced only locally by irradiation. Enhanced tumor selectivity is usually accomplished by immobilization of the photosensitizers in a designed drug delivery system. The covalent immobilization of the photosensitizer in a suitable nanoparticles system is an example and this may also prevent or attenuate prolonged skin sensitivity and facilitate clearance [Kumar et al., 2010; Sun, et al., 2009]. In this study, we utilized albumin nanoparticles to bind the photosensitizer. We hypothesized that, during delivery, self-quenching should reduce cytotoxic effects by accidental radiation. The nanoparticles were designed using a redox-sensitive crosslinker, and we hypothesized that they should disintegrate and thus eliminate the self-quenching only after uptake by the target cells (Figure 3.1).

3.2.1 HSA-Ce6-FA nanoparticles synthesis optimization

Several methods have been published to obtain protein nanoparticles. Even though the obtained nanoparticle size was appropriate for passive targeted drug delivery for cancer applications, a broad size distribution was observed. Langer and coworkers optimized a nanoprecipitation, or desolvation procedure to obtain nanoparticles with a narrow size distribution (Langer et al., 2003). The desolvation method consists of the dissolution of the HSA is 10 mM sodium chloride titrated to pH

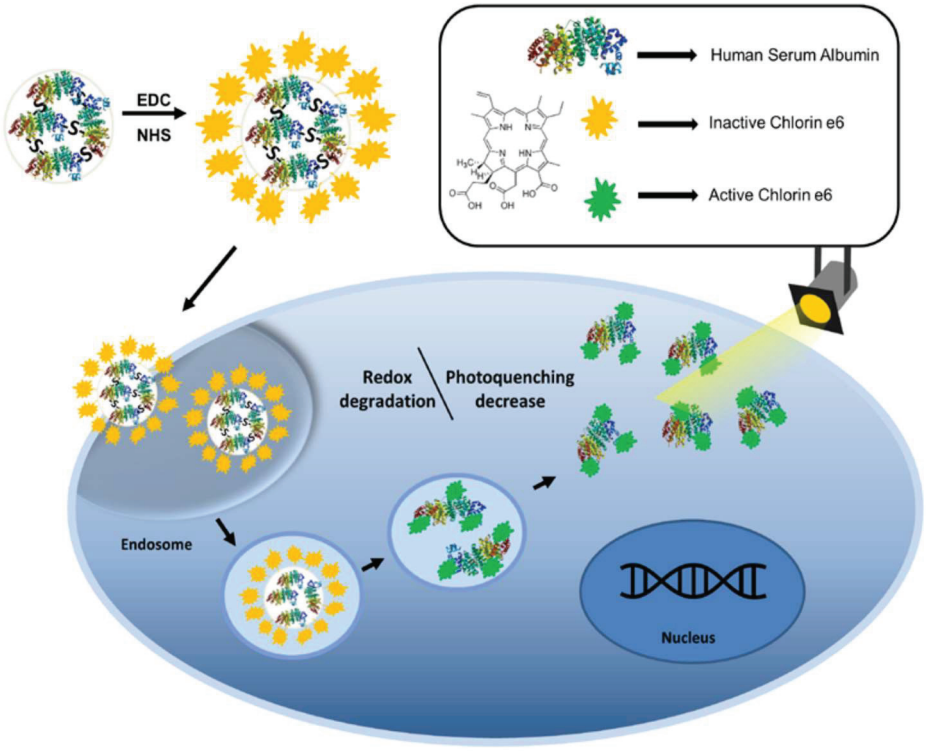

Figure 3.1 Representation of the redox-sensitive crosslinked photosensitizer-protein nanoparticles and possible cell uptake and activation routes.

9.0, and the subsequent addition of ethanol at a constant rate of 1 ml/min with constant stirring. The controlled addition of ethanol allows for the formation of transient nanoparticles in suspension. The high pH, far away from the HSA isoelectric point of 4.7, favors the formation of smaller particles in the suspension as a consequence of charge repulsions between the individual albumin proteins in solution. The nanoparticles formed must be stabilized by chemical crosslinking immediately after formation to prevent their dissolution after the removal of the organic solvent. Thus far, HSA nanoparticles had only been stabilized by the addition of glutaraldehyde, a homobifunctional crosslinker that reacts with primary amines [Langer et al., 2003, Chen et al., 2009]. This non cleavable crosslinker bond together the albumin proteins that make up the nanoparticle by reacting with the HSA lysines. Lysine residues are good candidates for chemical modifications since they are reactive functional groups that are typically available on the protein surface due to its polarity nature. Furthermore, primary amines are especially nucleophilic, compared to the other functional groups in proteins. HSA has 59 lysines available for potential modifications (Figure 3.2 (A)).

In order to introduce redox sensitivity, glutaraldehyde was substituted with dithiobis(succinimidyl propionate) (DSP), also known as Lomant's Reagent. This crosslinker also reacts on both ends with the primary amines in lysine, but bears a disulfide bond in its spacer arm (Figure 3.2 (B)). Hence, the crosslinker between the HSA proteins can be broken upon reduction. An additional difference is the size. The DSP crosslinker is significantly bigger in size than glutaraldehyde, so it is reasonable to expect

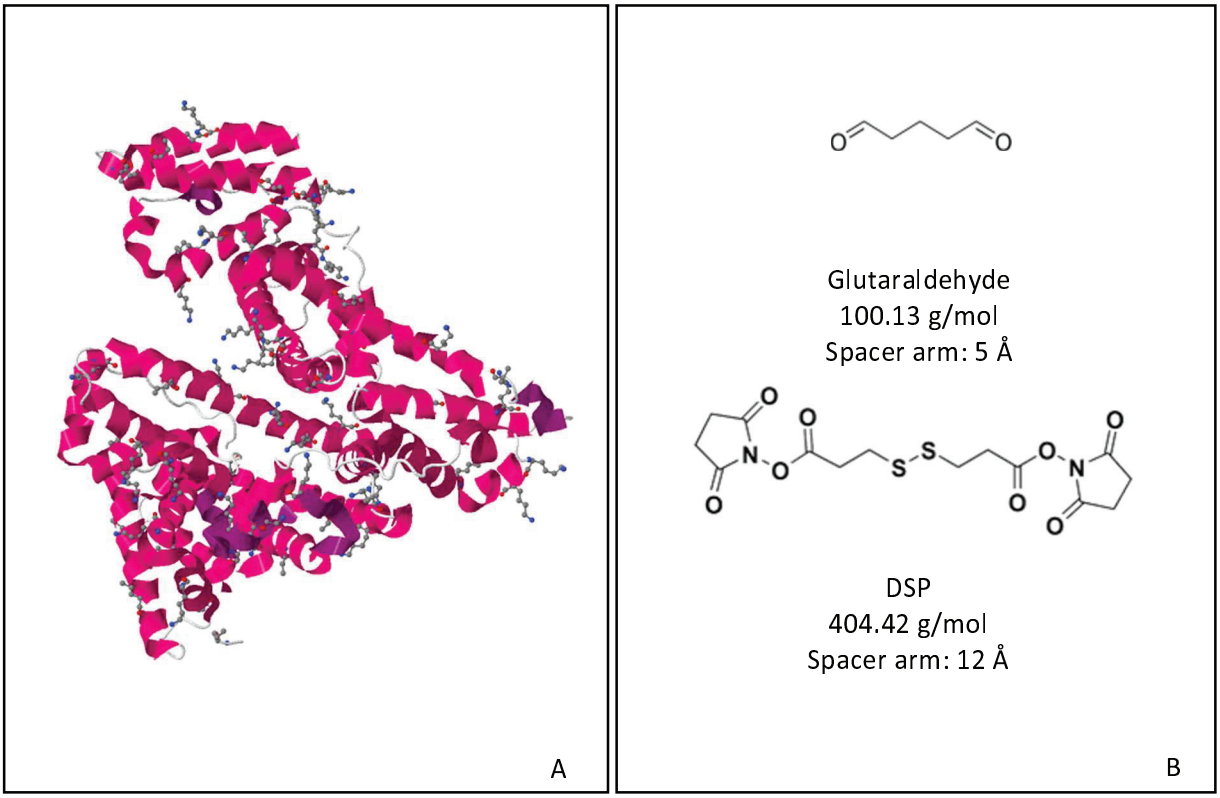

Figure 3.2 A: 3D crystalline structure of HSA complexed with cis-9-octadecenoid acid (Oleic acid), PDB entry: 1GNI, showing the 59 lysines in *ball and stick*. The lysines on the albumin surface are readily available for reactions. The primary amine on the lysine side chain has a pKa of 10.54, meaning that it has a positive charge at pH 9.0, used in the formation of HSA nanoparticles. B: Chemical structures of glutaraldehyde and DSP crosslinkers. Glutaraldehyde aggressive carbonyl (–CHO) reagents that condense amines via Mannich reactions and/or reductive amination. The carbon atom in the carbon-oxygen double-bond (C=O) is electrophilic and is very reactive towards nucleophiles such as primary amines. DSP contains an amine-reactive N-hydroxysuccinimide (NHS) at both ends. NHS esters react with primary amines at pH 7-9 to form stable amide bonds with the release of a N-hydroxy-succinimide leaving group. Additionally, DSP has a cleavable disulfide bond in its spacer arm, which results in redox sensitive crosslinking of the HSA that make up the nanoparticles.

the nanoparticle size and its structural rigidity to differ when using the different crosslinkers.

Even though the HSA nanoparticles synthesis by desolvation had been optimized by Langer and coworkers [2003], some of the conditions were initially changed. The use of acetone or acetonitrile was evaluated, but they resulted in the formation of big quantities of insoluble aggregates and very low yields (24.6 and 26.6%, respectively). Ethanol, on the other hand, produced very high yields as well as smaller monodisperse nanoparticles. The amount of ethanol added for desolvation was also changed, and a final water:ethanol ratio of 1:4 produced smaller nanoparticles. The crosslinking amount effect was evaluated and, in general, a higher amount of crosslinker did not significantly increase particle size. Table 3.1 summarizes the synthesis optimization results.

In this study, the model PS, Ce6 was covalently attached on the albumin nanoparticles surface by via EDC chemistry. The water-soluble EDC is a carbodiimide reacts with carboxylic acids in Ce6 to form an active O-acylisourea intermediate that is easily displaced by nucleophilic attack from primary amino groups. Sulfo-NHS was added to the EDC reaction to increase efficiency by stabilization of the intermediate. This allowed us to activate the Ce6 carboxylic acids, purify to remove excess reagents, and mix with the nanoparticle suspension, hence preventing the formation of by-products and increasing the protein modification efficiency. A higher drug immobilization ratio was attempted and up to 9 moles of Ce6 per mole of protein was covalently attached.

Table 3.1 Optimizations of the desolvation procedure to obtain HSA-Ce6 nanoparticles stabilized with glutaraldehyde or DSP

Synthetic conditions optimized		Radius (nm)	% Polydispersity	Observations
Desolvating agent	Acetone	113	23.6	Insoluble aggregates formed, low yield
	Acetonitrile	139	18.3	
	Ethanol	115	10.0	No aggregates observed
Water:ethanol ratio	1:.5	268	12.9	Higher addition of desolvating agent led to more stable suspensions.
	1:1	183	13.3	
	1:2	218	6.9	
	1:4	187	13.8	
Albumin concentration	25 mg/ml	249	11.3	50 mg/ml yielded the best size and polydispersity
	50 mg /ml	152	10.2	
	75 mg/ml	175	13.6	
Glutaraldehyde amount (% lysines crosslinked, stoichiometric ratio)	25 %	180	13.1	Small size changes were observed when the crosslinker amount was increased.
	50 %	212	7.3	
	75 %	220	9.0	
DSP amount (% lysines crosslinked, stoichiometric ratio)	25 %	165	7.8	
	50 %	169	8.9	
	75 %	180	13.2	

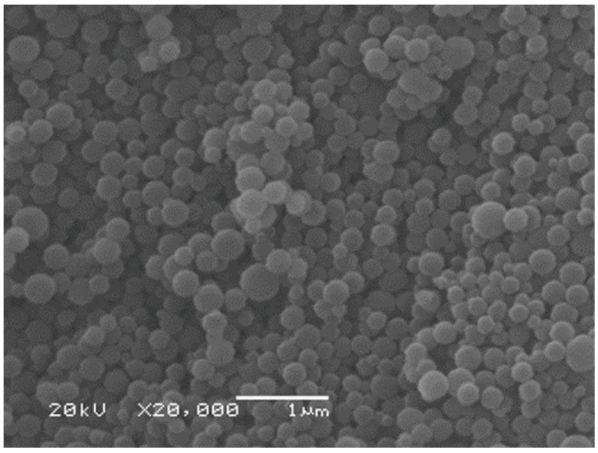

Figure 3.3 Scanning electron microscope (SEM) image of the HSA nanoparticle synthesized with the optimized conditions and crosslinked with glutaraldehyde showing that the general size, polydispersity and shape of the synthesized nanoparticle are appropriate.

Additionally, the nanoparticle purification was optimized. Washes with water and centrifugations were not enough to remove all the non-covalently attached Ce6, and this resulted in leaching of free Ce6 in solution. This leaching was detectable by UV-Vis absorption of the supernatant after nanoparticle centrifugation. Washes with ethanol were incorporated to the purification procedure. Three washes with ethanol were enough to remove all the adsorbed Ce6. UV-vis analysis of the supernatants against a Ce6 calibration curve at 400 nm (Ɛ= 173.97 ml/(mg·cm)) allowed for the quantification of the immobilized Ce6. After purification, the nanoparticles were washed with water for the removal of ethanol and subsequent lyophilization. The final procedure is represented in Figure 3.4.

The properties and SEM images of the final glutaraldehyde and DSP crosslinked nanoparticles used for all the subsequent experiments are summarized in Table 3.2 and shown in Figure 3.5. In general, no significant differences in size were observed between nanoparticles stabilized by the two crosslinkers, but an increase in polydispersity and negative surface zeta potential was produced when crosslinking with DSP instead of glutaraldehyde prior to immobilization of Ce6. The general characteristics of the synthesized system are similar to other albumin based nanoparticles previously reported [Langer et al., 2008].

3.2.2 Redox-responsive behavior of DSP crosslinked HSA-Ce6 nanoparticles

A critical examination of the DSP crosslinked Ce6-HSA nanoparticles consisted of exami-

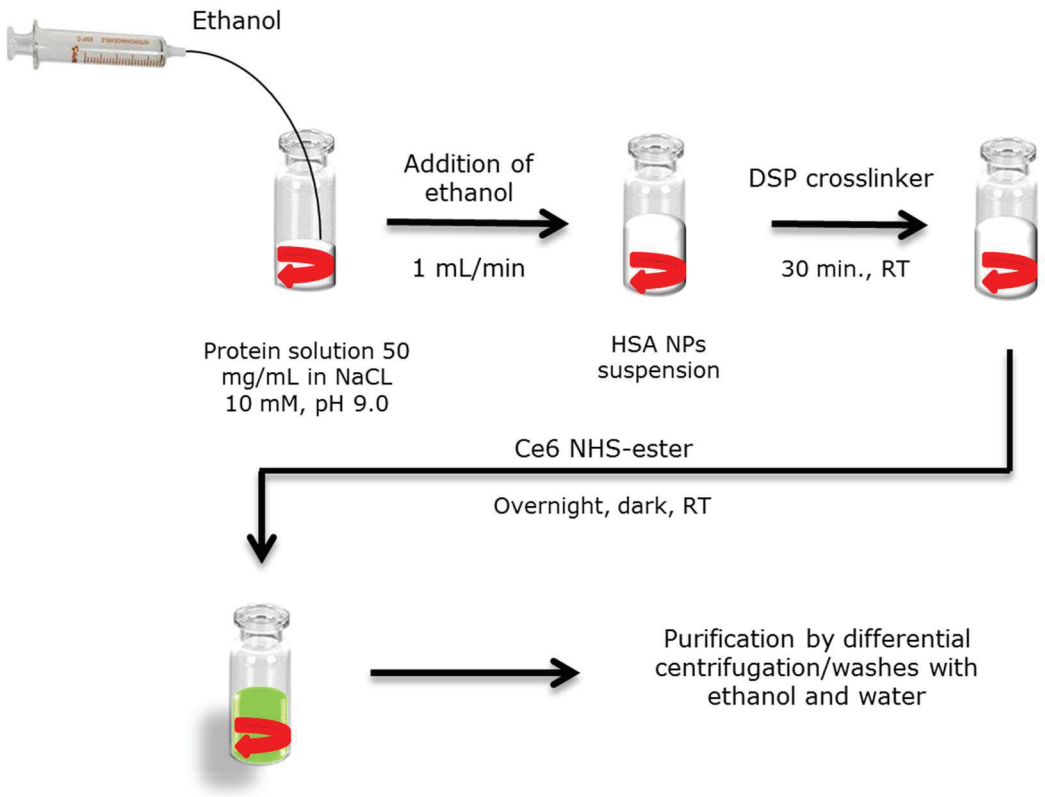

Figure 3.4 Final optimized synthetic procedure. The initial protein concentration was lowered to 25 mg/ml. Washes with ethanol were added to the purification steps to remove non covalently attached Ce6.

Table 3.2 Properties of the final nanoparticles synthesized and used in all subsequent experiments

Nanoparticle crosslinker	Diameter (nm)	Polydispersity Index	Zeta Potential (mV)	Ce6 loading (Ce6/HSA molar ratio)
Glutaraldehyde	298 ± 6	0.13 ± 0.01	-12.6 ± 0.3	9.6 ± 0.9
DSP	295 ± 5	0.24 ± 0.02	-18.0 ± 0.6	9.1 ± 0.7

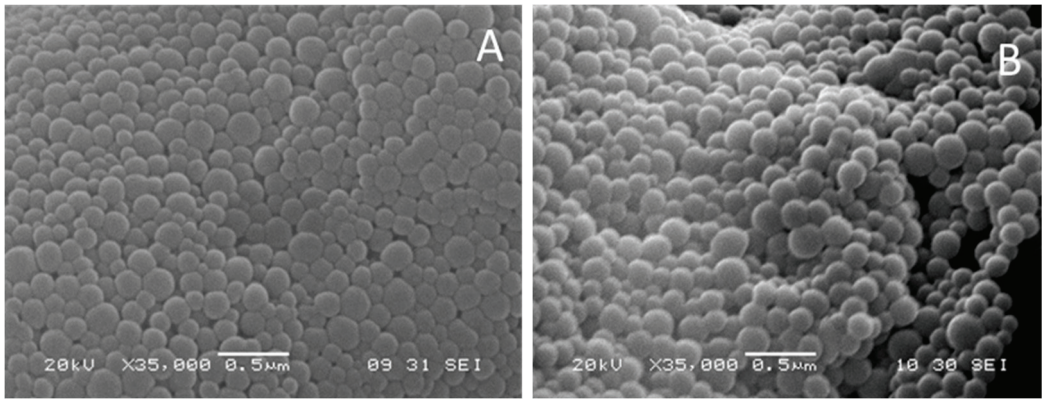

Figure 3.5 Scanning electron microscopy (SEM) images of HSA-Ce6 nanoparticles crosslinked with glutaraldehyde (A) and DSP (B).

ning whether they disintegrate in a reducing environment and if this would indeed result in a decrease in the photo quenching.

First, the crosslinking efficiency of DSP was determined by the TNBSA assay after nanoparticles dissolution by DTT. To test this, we synthesized three preparations of HSA nanoparticles varying the amount of crosslinking by using the DSP crosslinker at different concentrations. Under our conditions, the amount of amines modified per albumin molecule were 16, 24, and 35%, respectively, of the available amines, and the average DSP crosslinking efficiency was 65 ± 4%. These DSP crosslinked Ce6-HSA nanoparticles preparations were then examined for their ability to disintegrate in a reducing environment simulating the interior of cells. The Ce6-HSA nanoparticles were suspended in phosphate buffer containing 10 mM glutathione which corresponds to its concentration inside of cells [Winther and Jakob, 2013]. The turbidity of the suspensions was monitored by UV-vis absorption at 700 nm, where neither HSA or Ce6 absorb and all absorption can be attributed to turbidity. The decrease in turbidity is proportional to the nanoparticle disintegration. All of the Ce6-HSA nanoparticles stabilized using the redox responsive crosslinker exhibited a marked decrease in turbidity in the glutathione solution, while the glutaraldehyde crosslinked Ce6-HSA nanoparticles showed no decrease in turbidity (Figure 3.6). The amount of amines per albumin molecule modified with the redox-sensitive crosslinker increased proportionally to the amount of crosslinker added to the reaction. As expected, a higher modification degree resulted in a slightly increased stability in a reducing environment; hence, the nanoparticles took longer to break down. Because the nanoparticles with 15.5% of its amines crosslinked with DSP

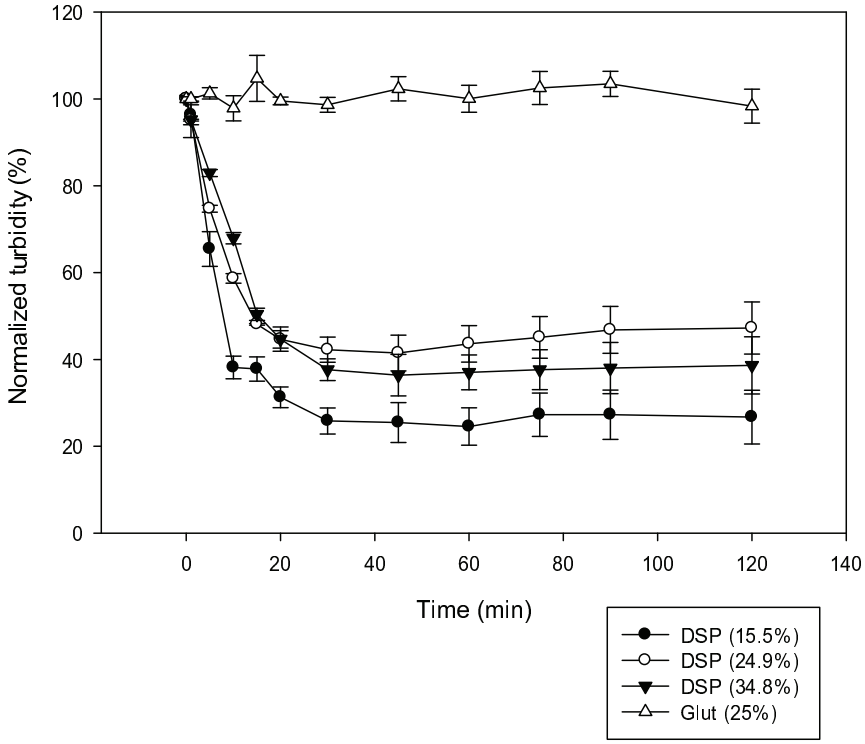

Figure 3.6 Dissolution profile of HSA nanoparticles crosslinked with glutaraldehyde of different amounts of DSP. The nanoparticles crosslinked with the least amount of DSP disintegrated quicker, and the glutaraldehyde crosslinked nanoparticles did not dissolve in a reducing buffer.

yielded the fastest disintegration while leaving a greater number of amines available for further reactions, this preparation was selected and used in all further studies.

Next, we investigated whether the disintegration of the nanoparticles after exposure to reducing agents would produce the expected decrease of Ce6 photo quenching. Non-chemical quenching of the photosensitizer fluorescence results in shorter fluorescence lifetimes and thus fluorescence yields. Thus, a reduction in quenching should cause an increase in the observed fluorescence emission under otherwise constant conditions. Indeed, we observed a decrease in fluorescence of the Ce6 after its immobilization in HSA nanoparticles, and an increase in the Ce6 fluorescence emission after nanoparticle incubation in a solution containing 10 mM glutathione (Figure 3.7). While no changes were observed for the glutaraldehyde crosslinked particles, particles crosslinked with the cleavable linker showed a decrease in particle size and an increase in fluorescence intensity upon establishing intracellular redox conditions.

Upon excitation (*hv*) of the photosensitizer intersystem crossing may occur resulting in the generation of ROS by two possible mechanisms. Type I reactions involve the formation of radical intermediates that transfer their energy to oxygen to form the superoxide anion radical (O_2^-) and the hydroxyl radical (OH•). Type II reactions consist in the transfer of energy from the photosensitizer excited state to the triplet ground state of molecular oxygen ($^3O_2$) to produce singlet oxygen ($^1O_2$). Because the lifetime of the triplet excited state (T1) is longer than that of the singlet state (S1), the type II mecha-

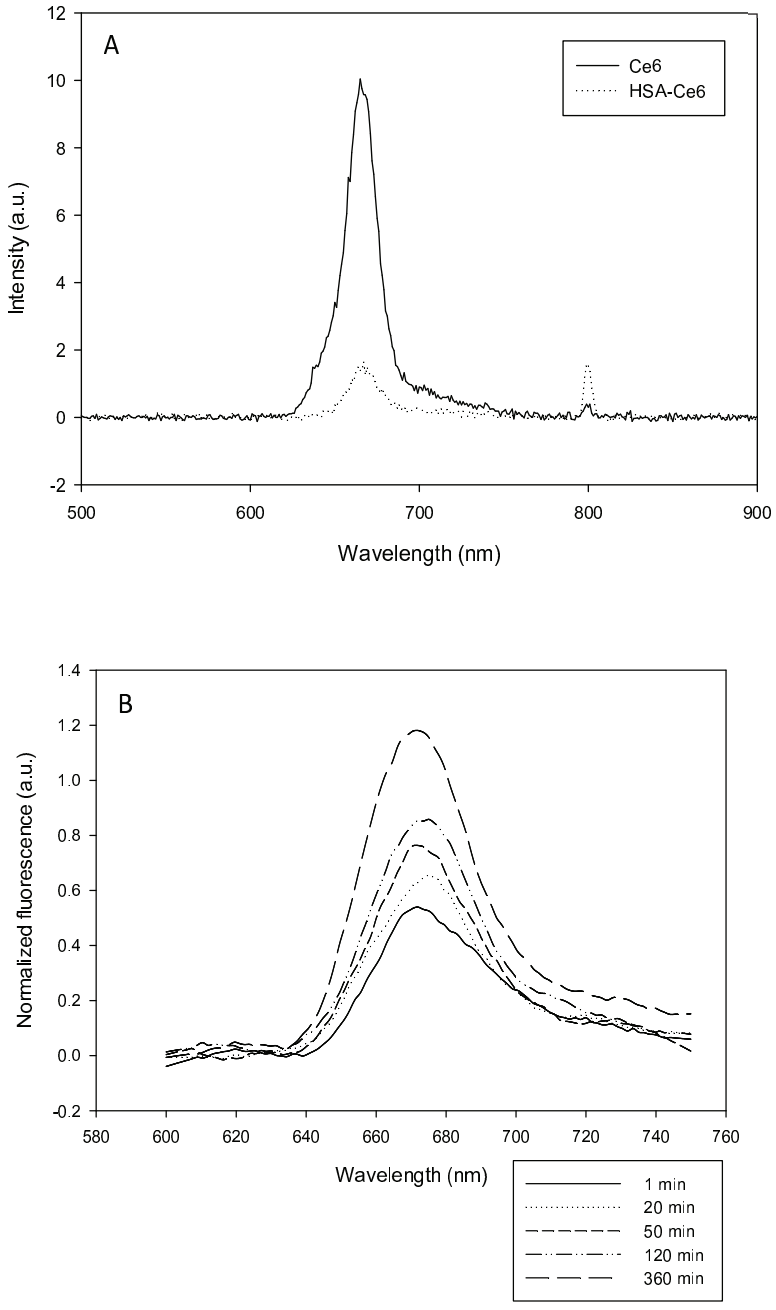

Figure 3.7 A: Emission spectra of free Ce6 and HSA-Ce6 nanoparticles adjusted to the same Ce6 concentration, excitation wavelength: 400 nm. The fluorescent emission of the Ce6 is largely quenched by immobilization in the HSA nanoparticles. B: Time dependent Ce6 photoquenching decrease in a reducing environment. DSP crosslinked HSA-Ce6 nanoparticles suspended in a glutathione 10 mM PBS solution showed increased fluorescence with time as a result of nanoparticle dissolution.

nism typically predominates. Even though tumor destruction by PDT is complex (including apoptosis and necrosis, as well as induction of immunological responses and destruction of the tumor vasculature), singlet oxygen is considered the main cytotoxic agent (Gomer, 2010). In order to determine whether the observed photo quenching decrease would effectively translate into an increased ROS production, specifically of singlet oxygen, following irradiation, a proof-of-concept experiment was performed.

To test for singlet oxygen production of the Ce6-HSA nanoparticles after exposure to reducing and non-reducing conditions, the p-nitrosodimethylaniline (RNO) bleaching method was used. Both glutaraldehyde and DSP crosslinked Ce6-HSA nanoparticles were used to bleach RNO in PBS in a non-reducing medium and after being exposed to a reducing medium for 18 h. Unconjugated Ce6 was used as an additional control in this set of experiments. Our data show that the covalent attachment of Ce6 to the nanoparticles effectively prevented the generation of singlet oxygen because no significant bleaching of the dye occurred (Figure 3.8). In contrast, the control consisting of free Ce6 produced the highest decrease in absorbance of RNO as result of copious singlet oxygen generation. Importantly, when the smart nanoparticles were exposed to reducing agents and disintegrated, the singlet oxygen generation increased to approximately half of the value produced by the free Ce6. Glutaraldehyde crosslinked nanoparticles did not show such a significant increase in singlet oxygen production when exposed to reducing conditions. This highlights a desirable characteristic of a smart drug delivery system for photosensitizers: prevention of premature toxicity even upon (accidental) premature irradiation. Our system clearly fulfills this requirement.

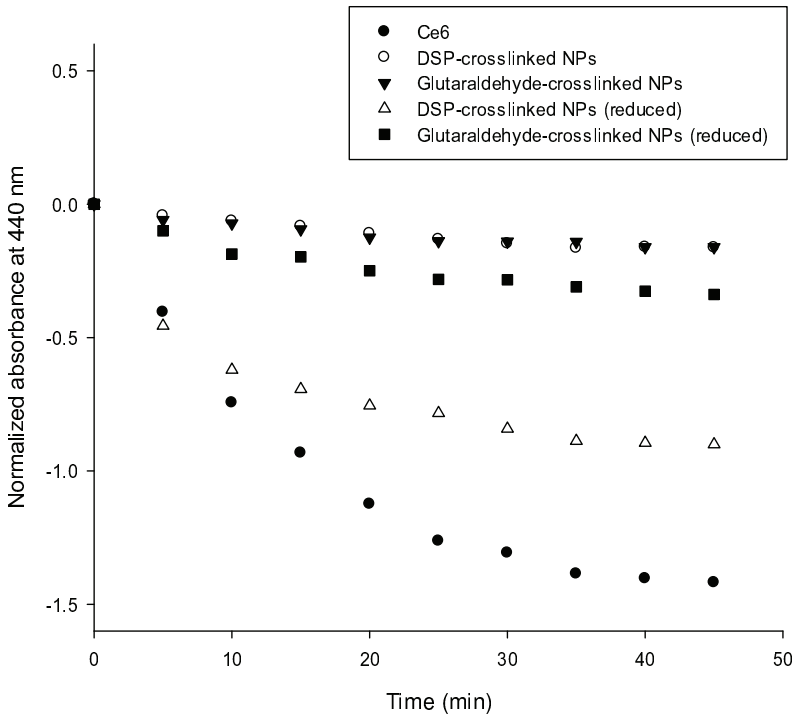

Figure 3.8 Spectrophotometric assay for the determination of singlet oxygen generation by the Ce6-HSA nanoparticles formulations after incubation in 10 mM and 0.001 mM glutathione for 18 h. Upon generation of singlet oxygen as a result of irradiation, the RNO absorbance at 440 nm is bleached. Only the reduced DSP crosslinked nanoparticles are able to partially restore the singlet oxygen generation of the free Ce6.

3.2.3 Dark and photo-toxicity

Even though a drug delivery system is expected to minimize nonselective cell internalization, the targeting of healthy cells is always a concern. To address this issue we tested the dark toxicity (cell viability without irradiation) of the photosensitizer-protein nanoparticles and the free drug in HeLa cells (cervical cancer), A549 (lung cancer) and human umbilical vein endothelial cells (HUVEC), a normal (non-cancer) cell line. The results show that even at the lowest concentration tested the free drug caused some toxicity, which was significantly reduced by the drug immobilization in the HSA nanoparticles. The free drug dose toxic effect was more evident in the normal cell line tested (Figure 3.9). Neither the glutaraldehyde nor the DSP crosslinked nanoparticles caused significant decrease in cell viability at any concentration tested by us. These results are further evidence of the advantage of placing the photosensitizer in a delivery system instead of administering the free drug. It is possible that the system selectivity towards specific cell types can be further enhanced by modifying the nanoparticles surface with a targeting ligand.

Next, we wanted to investigate the cell death induction by nanoparticle-mediated PDT. For this purpose, HeLa cells were treated with both the glutaraldehyde and the DSP crosslinked Ce6-HSA nanoparticles, adjusted to a drug concentration of 5 ng/ml. After 24 hours of incubation, the co-localization of DAPI and PI was determined.

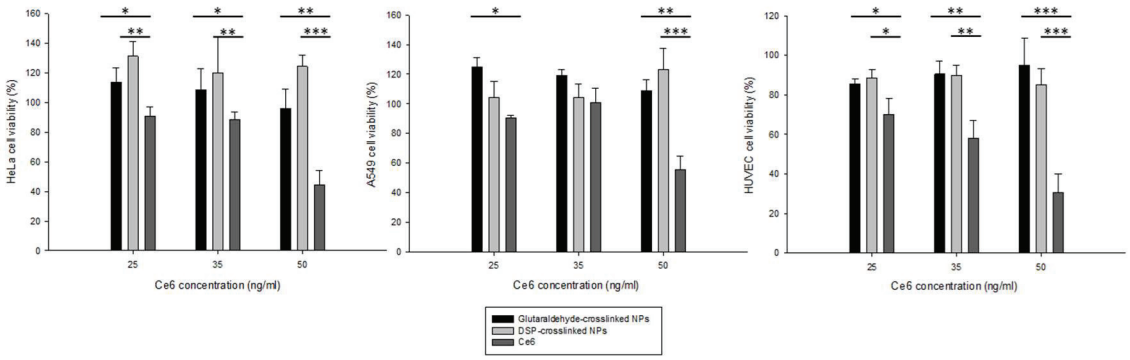

Figure 3.9 Dark toxicity in HeLa cells (A) A549 (B) and HUVEC cells (C) of the glutaraldehyde crosslinked nanoparticles, the DSP crosslinked nanoparticles, and the free Ce6 at different drug concentrations after a 24 hours of incubation. Asterisks indicate statistical significance with *p<0.05, **p<0.001, and ***p<0.0001.

The PI internalization is representative of highly condensed and fragmented chromatin in apoptotic cells characteristic of late apoptosis, as well as necrosis induction (Morales et al., 2014). Our results confirm qualitatively that, after exposure to light, both drug-containing nanoparticles induce cell death (Figure 3.10). It is also possible that some necrosis is induced as well at this drug concentration and light fluence. In contrast, untreated cells presented no indication of any form of cell death, as can be observed by the lack of intense red fluorescence due to PI internalization. At the concentrations tested, caspase-3 dependent apoptosis was not identified (Table 3.3).

3.2.4 Dose and time-dependent phototoxicity

In order to quantitatively determine the cell viability difference between the glutaraldehyde and the DSP crosslinked Ce6-HSA nanoparticles, dose-response curves were constructed after incubation for 1, 6, and 24 hours. All cells were irradiated to induce phototoxicity immediately after incubation. After 1 and 6 hours of incubation, no significant difference was observed between the death inductions by either type of Ce6-HSA nanoparticles. However, after 24 hours of incubation, a statistically significant difference between the Ce6-HSA nanoparticles with the different crosslinkers was apparent (Figure 3.11). The DSP crosslinked Ce6-HSA nanoparticles were able to decrease the cell viability by at least 20% more than the glutaraldehyde crosslinked nanoparticles in the 5-15 ng/ml Ce6 concentration range. Even though both types of Ce6-HSA nanoparticles showed an increase in death induction with longer incubation times,

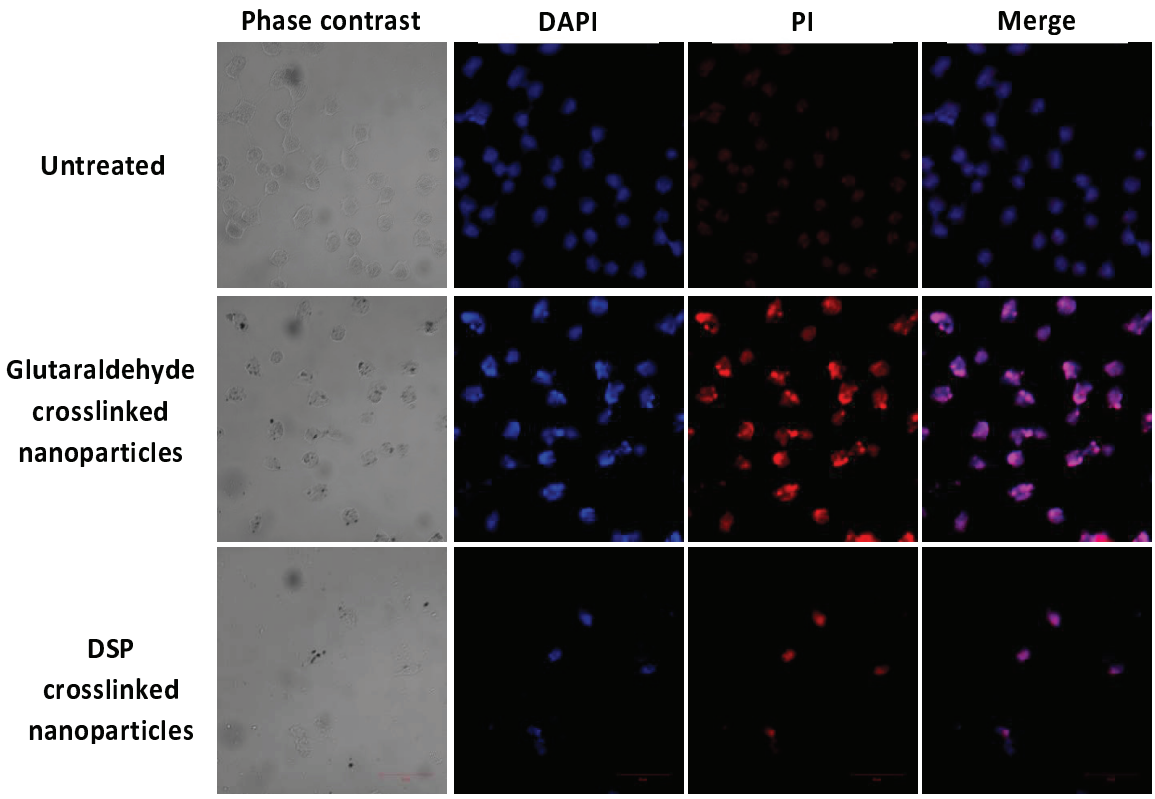

Figure 3.10 DAPI/PI-stained cells examined by confocal microscopy. The treated cells were incubated for 24 hours with either the glutaraldehyde or the DSP crosslinked Ce6-HSA nanoparticles and irradiated with a 660 nm LED lamp for 10 minutes. The images show that both types of HSA-Ce6 nanoparticles cause cell death.

Table 3.3 Caspase-3 activation in HeLa cells by dark and irradiated Ce6 and HSA-Ce6 nanoparticles

p-nitroaniline absorbance intensity at 405 nm	Caspase-3 Positive Control	Ce6 0.01 mg/ml	HSA-Ce6 nanoparticles 0.1 mg/ml
dark	0.53 ± 0.02	0.07 ± 0.03	-0.01 ± 0.08
irradiated	0.448 ± 0.009	0.11 ± 0.03	0.05 ± 0.01

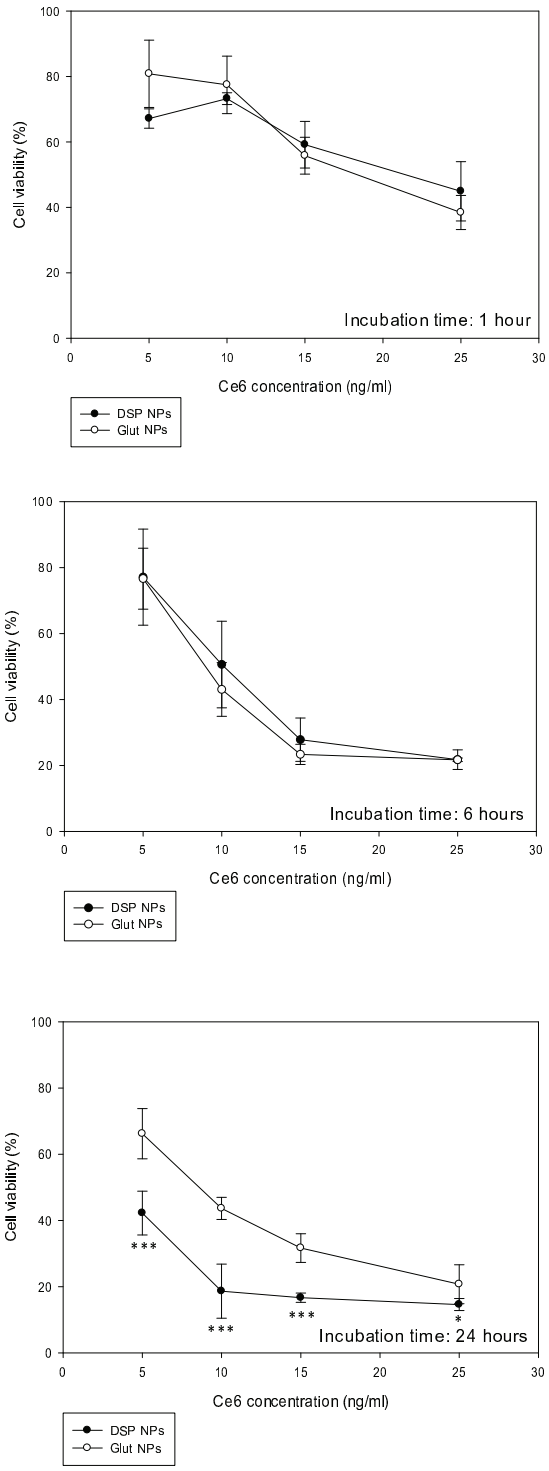

Figure 3.11 HeLa cell viability after incubation with glutaraldehyde or DSP crosslinked nanoparticles as a function of the Ce6 concentration after 1, 6, and 24 hours of incubation. Two-tailed t-test was used to establish significance at each individual time point; Asterisks indicate statistical significance with *p<0.05 and ***p<0.0001.

possibly due to proteolytic degradation of the nanoparticles leading to drug activation, the DSP crosslinked nanoparticles were much more efficiently activated by 24 hours of incubation. This result indicates an improvement in the drug delivery function mediated by redox-sensitivity, particularly after longer dose-light intervals and at lower concentrations.

3.2.5 HSA-Ce6 nanoparticles cell uptake and intracellular fate

Next, we wanted to qualitatively evaluate the internalization mechanism and time-dependent localization of the nanoparticles within the HeLa cells. For this purpose, we labeled both types of nanoparticles with amine-reactive fluorescein isothiocyanate (FITC) and co-incubated them with FM4-64, an endosomal marker. The drug concentration was adjusted to 10 ng/ml and the cells were not exposed to light to prevent photo toxicity. After 6 hours of incubation, both the glutaraldehyde and the DSP crosslinked Ce6-HSA nanoparticles, appear to be co-localized with endosomes (Figure 3.12). After 24 hours, however, the fluorescence was distributed evenly throughout the cell. Both the redox-sensitive and the redox insensitive nanoparticles appeared to be equally internalized and behaved similarly after 6 and 24 hours of incubation. The substitution of glutaraldehyde with DSP did not alter the nanoparticle internalization or its intracellular fate. Also, the images show that the nanoparticles are able to escape the endosome, which is a necessary condition to reach the glutathione-rich cytosol. This endosomal escape occurs after 6 hours of incubation, which possibly explains the quantitative differences in cytotoxicity induced after 24 hours of incubation.

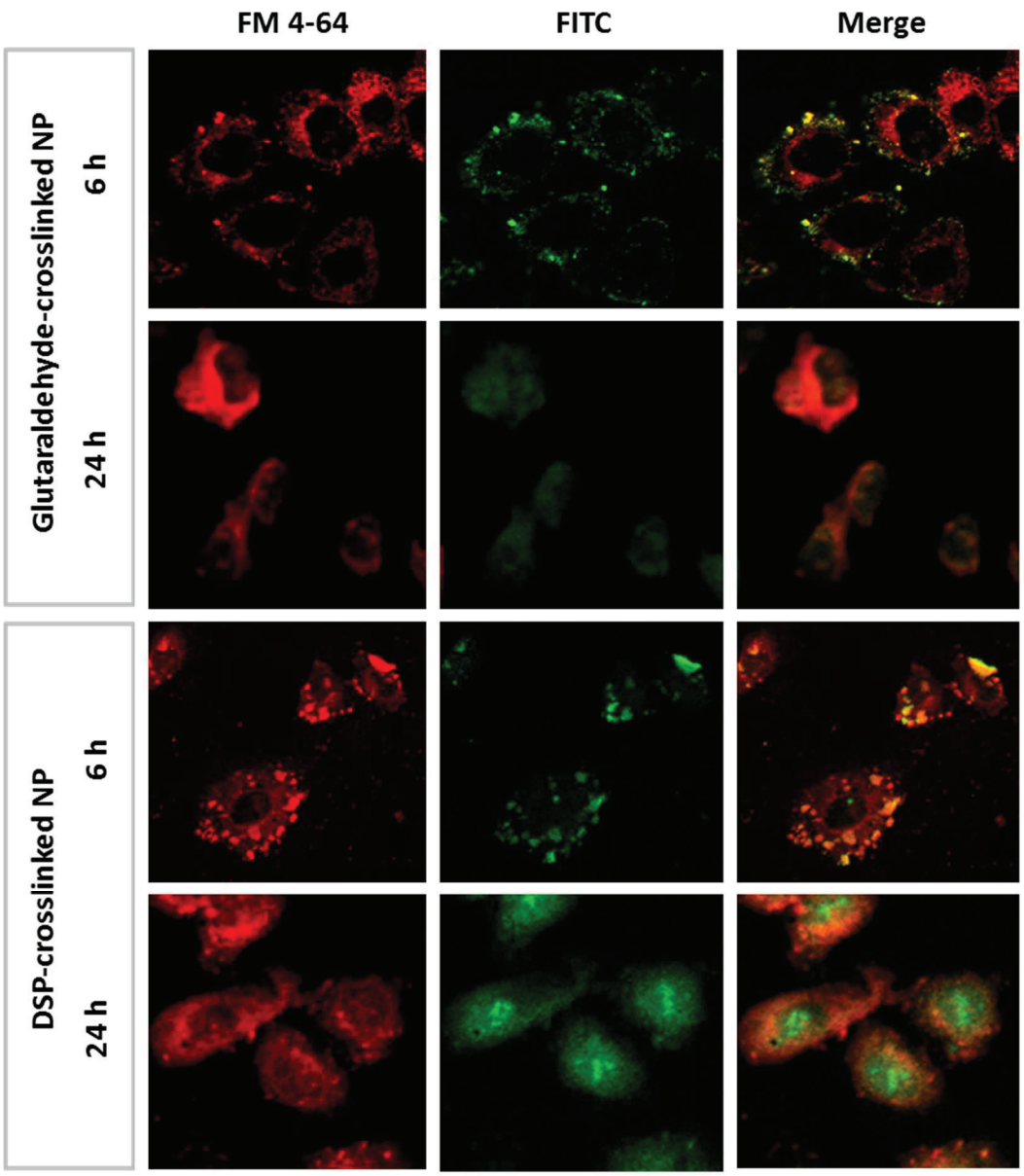

Figure 3.12 Qualitative examination of the endosomal escape of glutaraldehyde and DSP crosslinked HSA-Ce6 nanoparticles in HeLa cells by confocal microscopy. The cells were incubated with the nanoparticles adjusted to a drug concentration of 10 ng/ml for 6 hours and were not exposed to light. Images show the cells incubated with FM-4-64 to label the endosomes, the cells exposed to FITC-labeled nanoparticles, and the merged image.

3.3 Conclusions

We designed and synthesized a smart redox-responsive system for PDT by stabilizing albumin nanoparticles using a thiol-cleavable crosslinker. The obtained nanoparticles had a suitable size, shape, and polydispersity to theoretically allow for tumor targeting. The fluorescence of the immobilized model photosensitizer Ce6 was successfully quenched when the nanoparticles were intact, and the quenching was shown to be inversely proportional to the generation of singlet oxygen, the main phototoxic agent of PDT. The designed system successfully prevented dark toxicity in healthy or non-targeted tissues, as shown *in vitro*. Furthermore, singlet oxygen production was low when the nanoparticles were intact. Nanoparticles disintegration produced by reducing conditions caused increased singlet oxygen production and resulted in increased cell death upon radiation. Redox-sensitive crosslinking of the Ce6-HSA nanoparticles did not alter interactions with the cells in terms of internalization routes and subcellular localization. Altogether, our results provided evidence that our designed redox-responsive system is significantly more efficient in inducing cell death after longer dose-light intervals than the non-redox responsive nanoparticles. Finally, this work provides a working model of how to improve existing tumor-targeted nanoparticle-based PDT.

3.4 Bibliography

Allison, R. R.; Mota, H.C.; Bagnato, V.S.; Sibata, C.H. Bio-nanotechnology and photodynamic therapy-state of the art review. *Photodiagnosis Photodyn. Ther.* **2008**, *5*, 19-28.

Allison, R. R. Photodynamic therapy: oncologic horizons. *Future Oncol.* **2014**, *10*, 123-124.

Chen, K.; Preuß, A.; Hackbarth, S.; Wacker, M.; Langer, K.; et al. Novel photosensitizer-protein nanoparticles for photodynamic therapy: photophysical characterization and in vivo investigations. *Photochem. Photobiol. B.* **2009**, *96*, 66-74.

Giuntini, F.; Alonso, C. M. A.; Boyle, R. W. Synthetic approaches for the conjugation of porphyrins and related macrocycles to peptides and proteins. *Photochem. Photobiol. Sci.* **2011**, *10*, 759-791.

Gomer, C. J. *Photodynamic Therapy Methods in Molecular Biology*; Humana Press: New York, 2010.

Kratz, F. Albumin as a drug carrier: design of prodrugs, drug conjugates and nanoparticles. *J. Control. Release*. **2008**, *132*, 171-183.

Kumar, R.; Roy, I.; Ohulchanskky, T. Y; Vathy, L. A.; Bergey, E. J.; et al. In vivo biodistribution and clearance studies using multimodal organically modified silica nanoparticles. *ACS Nano.* **2010**, *4*, 699-708.

Langer, K.; Anhorn, M. G.; Steinhauser, I.; Dreis, S.; Celebi, D.; et al. Human serum albumin (HSA) nanoparticles: reproducibility of preparation process and kinetics of enzymatic degradation. *Int. J. Pharm*. **2008**, *347*, 109-117.

Langer, K.; Balthasar, S.; Vogel, V.; Dinauer, N.; von Briesen, H.; et al. Optimization of the preparation process for human serum albumin (HSA) nanoparticles. *Int. J. Pharm*. **2003**, *257*, 169-180.

Li, L.; Hitchcock, A. P.; Cornelius, R.; Brash, J. L.; Scholl, A.; et al. X-ray microscopy studies of protein adsorption on a phase segregated polystyrene/polymethyl-methacrylate surface. 2. Effect of pH on site preference. *J. Phys. Chem. B*. **2008**, *112*, 2150-2158.

Morales-Cruz, M.; Figueroa, C. M.; González-Robles, T.; Delgado, Y.; Molina, A.; et al. Activation of caspase-dependent apoptosis by intracellular delivery of Cytochrome c-based nanoparticles. *J. Nanobiotechnology*. **2014**, *12*, 33.

Philchenkov, A. A.; Shishko, E. D.; Zavelevich, M. P.; Kuiava, L. M.; Miura, K.; et al. Photodynamic responsiveness of human leukemia Jurkat/A4 cells with multidrug resistant phenotype. *Exp. Oncol.* **2014**, *36*, 241-245.

Preuss, A.; Chen, K.; Hackbarth, S.; Wacker, M.; Langer, K.; et al. Photosensitizer loaded HSA nanoparticles II: in vitro investigations. *Int. J. Pharm*. **2011**, *404*, 308-316.

Schroeder, A.; Heller, D. A.; Winslow, M. M.; Dahlman, J. E.; Pratt, G. W.; et al. Treating metastatic cancer with nanotechnology. *Nat. Rev. Cancer*. **2011**, *12*, 39-50.

Sun, Y.; Chen, Z. L.; Yang, X.X.; Huang, P.; Zhou, X. P.; et al. Magnetic chitosan nanoparticles as a drug delivery system for targeting photodynamic therapy. *Nanotechnology*. **2009**, *20*, 135102.

Torchilin, V. Tumor delivery of macromolecular drugs based on the EPR effect. *Adv Drug Deliv Rev*. **2011**, *63*, 131-135.

Wacker, M.; Chen, K.; Preuss, A.; Possemeyer, K.; Roeder, B.; et al. Photosensitizer loaded HSA nanoparticles. I: Preparation and photophysical properties. *Int. J. Pharm*., **2010**, *393*, 253-262.

Winther, J. R.; Jakob, U. Redox control: A black hole for oxidized glutathione. *Nat. Chem. Biol*. **2013**, *9*, 69-70.

Chapter 4

Higher Apoptosis Induction by the Co-delivery of Cytochrome c and a Photosensitizer in a Single Nanoparticle

4.1 Summary

Cancer remains one of the most difficult diseases to treat and cure due to its heterogeneity. Since a single tumor can contain cells with many different mutations, using a single drug is not efficient enough. In fact, currently most patients are treated with a combination of two or more drugs administered simultaneously. Typically, combinations of small chemotherapeutic drugs are used [Frei and Eder, 2003]. These potent cocktails may attack different targets or act synergistically, which increases therapeutic strength and temporarily overcomes multidrug resistance [Ghavami et al., 2011].

The identification of new treatments and the combination of some of them may represent a significant improvement to the clinical tools currently used. In this work we describe the design and optimization of a redox-sensitive protein-drug bioconjugate nanoparticle system. The designed system co-delivers a protein and a photosensitizer (PS) drug as a model for cancer combination therapy. Co-delivery within a single delivery system represents a significant improvement to free drug concurrent administration, since all drugs have different pharmacokinetic and biodistribution profiles, and may not reach the target tissue simultaneously in the desired proportions [Jian et al., 2014].

Uniting different therapeutic agents into a single nano-platform can help regulate and enhance combination therapies.

The protein used in our model is Cytochrome c (Cyt c), a pro-apoptotic protein that activates caspase dependent apoptosis when it is in the cell cytoplasm by interacting with Apaf-1 to form the apoptosome [Cai et al., 1998]. In general, intracellular protein delivery is challenging; it requires the passage across the plasma membrane, and the escape from the endosomes after internalization [Fu et al., 2014]. Cyt c has been delivered into cells by its immobilization in nanocarriers, such as mesoporous silica nanoparticles (MSN) [Méndez et al., 2014], a dendritic supramolecular delivery system [Ng et al., 2013], polymeric nanoparticles [Santra et al., 2010] or by its coupling with galactosylated albumin, which targets a highly expressed receptor in hepatocarcinoma [Yeh et al., 2014]. In previous works, we have successfully synthesized a protein delivery system with Cyt c as its core [Morales-Cruz et al., 2014, Morales-Cruz et al., 2016]. The Cyt c-based nanoparticle core was synthesized by the desolvation method. In this dissertation, we use this method to obtain Cyt c nanoparticles that were subsequently stabilized with the redox-sensitive Dithiobis(succinimidyl propionate) (DSP) crosslinker. Our aim was to obtain transiently insoluble nanoparticles that can dissolve in the intracellular environment, releasing the active protein [Xu et al., 2012].

The Cyt c nanoparticle surface was decorated with the photosensitizer drug Ce6 to accomplish co-delivery of the pro apoptotic protein and the drug. The photosensitizer acts by generating reactive oxygen species that cause cell death upon irradiation. Previous

research has shown that free Ce6 associates with carrier proteins during delivery, and that its internalization in the cell depends on the protein. However, when the Ce6 is not covalently immobilized, it localizes in the plasma membrane and in intracellular vesicles [Mojzisova et al., 2007]. In our system, the Ce6 is never released, as it is covalently attached to the Cyt c.

Previous research indicate that high dose PDT is predominantly associated with the induction of necrosis, whereas low dose PDT correlates with increased induction of apoptosis [Almeida et al., 2004]. Interestingly, a study reports that low dose PDT with Ce6 significantly sensitizes TRAIL-resistant cancer cells to TRAIL-induced apoptosis [Szliszka et al., 2011]. TRAIL (tumor necrosis factor-related apoptosis inducing ligand) is a death ligand that induces apoptosis by the activation of death receptors [Holoch and Griffith, 2009]. In this study, we aim at determining if cell apoptosis can be enhanced by co-delivery of Cyt c and Ce6.

Reiners and coworkers [2002] demonstrated that N-aspartyl Chlorin e6, which localizes in the lysosome, disrupts the lysosomal membrane upon irradiation. This results in the cleavage of Bid, a pro apoptotic member of the Bcl-2 supergene family, and the subsequent mitochondrial apoptotic pathway activation. If the Ce6 in our system exhibits a similar behavior, we hypothesize that our system can enhance the pro apoptotic capacity of Cyt c nanoparticles by inducing the release of the cell's endogenous Cyt c.

Herein, we developed a protein-drug bioconjugate nanoparticle that is effectively internalized by the cell *in vitro* to release its therapeutic payload. The designed drug

delivery system (DDS) is hypothesized to be selective towards cancer tissue *in vivo* though passive targeting due to its size. Also, this DDS is only effective upon uptake into the reducing intracellular environment due to the redox-sensitive crosslinking, which is hypothesized to trigger the protein release and activate the photosensitizer action by decrease of the photoquenching [Molina et al., 2015] (Figure 4.1). This study focuses only on the function of the therapeutic agents when administered together, and does not incorporate an active targeting strategy.

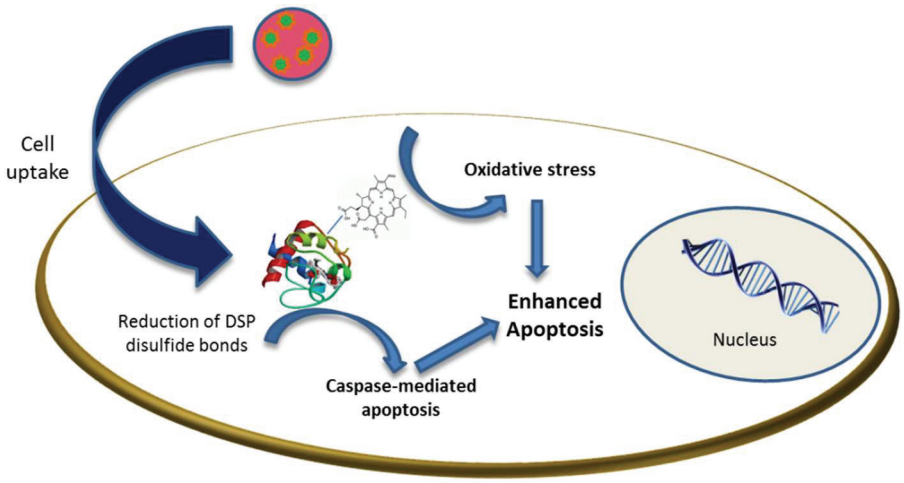

Figure 4.1 Scheme showing the hypothesized therapeutic strategy. Upon nanoparticle internalization, it dissolves into Cyt c protein monomers to induce caspase-mediated apoptosis in the cytosol. The Ce6 immobilized in some of the Cyt c produces reactive oxygen species after irradiation, affecting the mitochondrial membrane integrity and inducing the release of endogenous Cyt c, effectively augmenting the intrinsic apoptotic signal.

4.2 Results and Discussion

4.2.1 Preparation and optimization of protein-drug nanoparticles

The desolvation method used previously by us was optimized to obtain Cyt c NP [Morales-Cruz et al., 2014]. The nanoparticles were formed though the controlled addition of acetonitrile to form a suspension, followed by covalent crosslinking with DSP, a homobifunctional crosslinker that has a disulfide bond in its arm. This results in stable nanoparticles that only dissolve into Cyt c monomers upon exposure to reducing agents such as glutathione (GHS), the most abundant reducing agent in the cytosol (Figure 4.2). The process to obtain Cyt c nanoparticles stabilized by DSP of an appropriate size and polydispersity was optimized first. The addition of methyl-ß-cyclodextrin (mßc) as excipient was initially evaluated. Cyclodextrins are a common stabilizing excipient used in drug delivery (Strickley, 2004). Three different Cyt c:mßc ratios were tested (1:2, 1:4 and 1:10) (Figure 43). All combinations of Cyt c with mßc yielded nanoparticles with good polydispersity and morphology. However, their size was bigger than expected (0.8 to 1 µm) (Figure 4.3). Next, the synthesis was attempted without the addition of excipients. Different Cyt c concentrations were tested (5, 10, and 25 mg/ml). The Cyt c concentration of 10 mg/ml was selected for all further studies using as criteria the yield, and the particle size and polydispersity (Figure 4.4, Table 4.1).

The Cyt c crosslinking with a redox-sensitive crosslinker provides the nanoparticle with the ability to dissolve in the cell cytosol. The crosslinking extent was optimized to ensure proper stabilization and appropriate release in a reducing environment. Initially, a stoichiometric ratio to crosslink 50% of the 19 available lysines

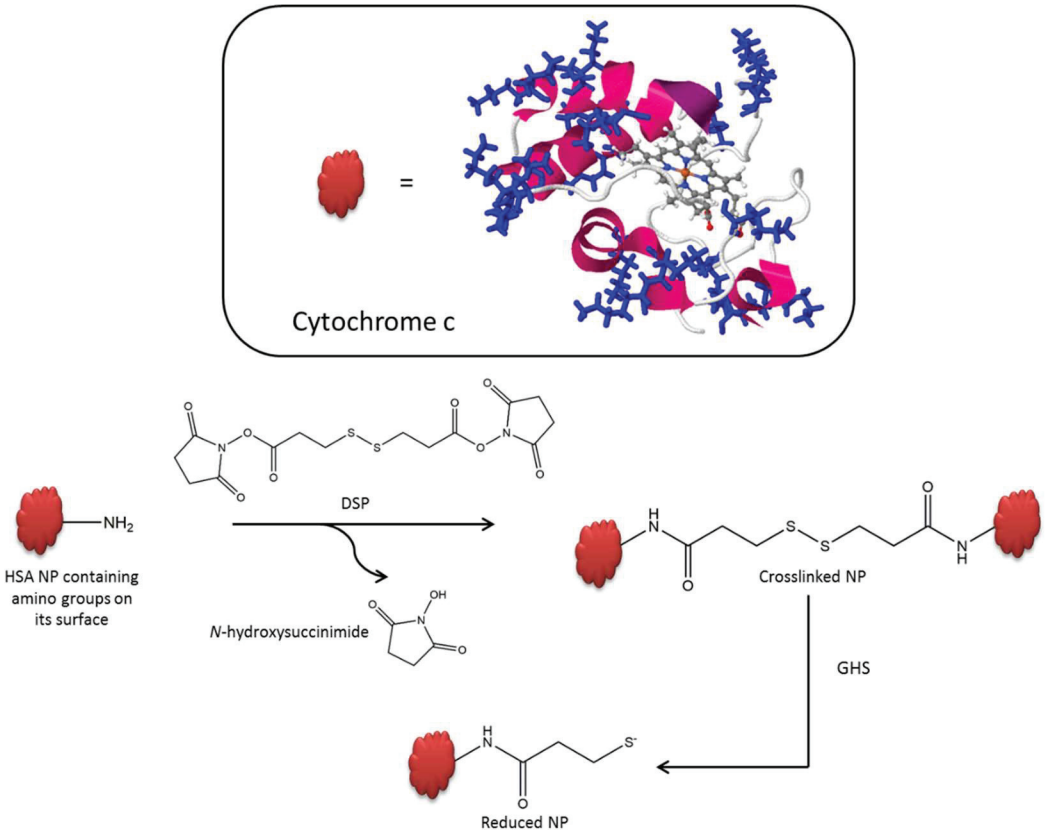

Figure 4.2 Crosslinking reaction of the Cyt c nanoparticle (NP) surface by DSP and subsequent nanoparticle disintegration upon exposure to reducing agents in the cell cytosol such as glutathione (GHS). The 3-dimensional Cyt c structure shows the 19 lysine residues available for reaction in blue.

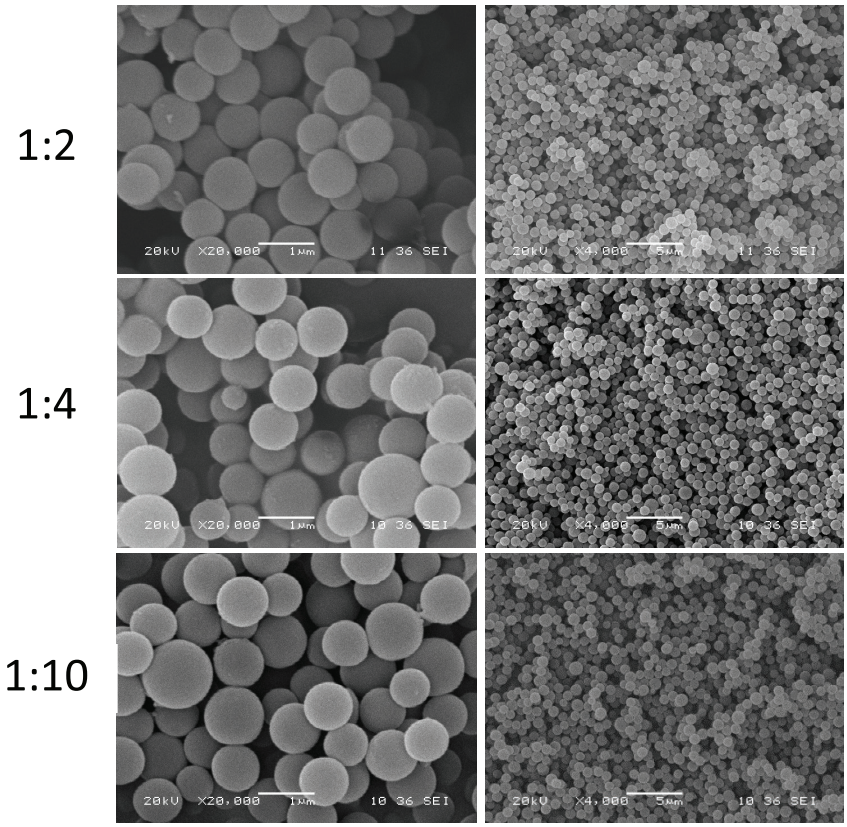

Figure 4.3 Cyt c NP synthesized by the desolvation method using acetonitrile as the desolvating agent and methyl-ß-cyclodextrin (mßc) as excipient. The protein:mßc ratios used were 1:2, 1:4 and 1:10. All the resulting NP exhibited good spherical morphology and monodispersity, but the size was bigger than expected.

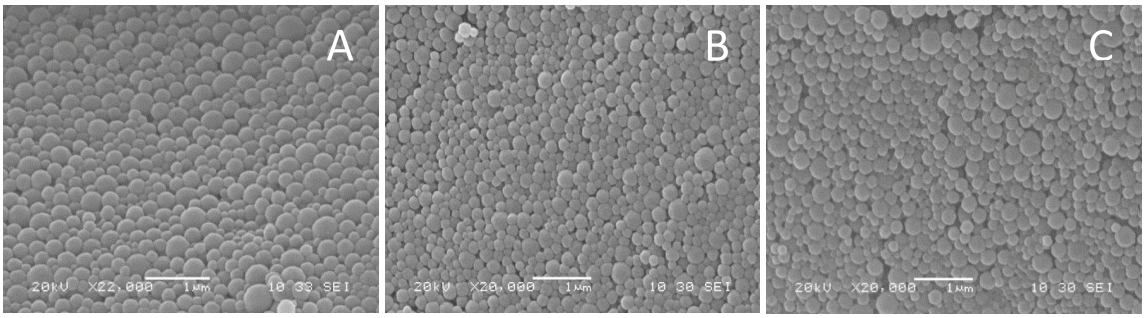

Figure 4.4 SEM images of Cyt c NP synthesized with different initial protein concentrations: 5 mg/ml (A), 10 mg/ml (B), 25 mg/ml (C).

Table 4.1 Properties of the nanoparticles synthesized with different initial protein concentrations. These criteria were used to select the optimized protein concentration used for all further experiments: 10 mg/ml.

Sample	Insoluble aggregates (%)	Nanoprecipitation efficiency	Hydrodynamic Diameter (nm)	PDI
5 mg/ml	1.2	93.6	343 ± 25	0.35 ± 0.06
10 mg/ml	4.4	94.4	304 ± 15	0.3 ± 0.1
25 mg/ml	4.6	94.7	373 ± 14	0.395 ± 0.005

in Cyt c was added. Even though the particle size was not affected by the addition of different amounts of cross-linker, the release profile was. This crosslinking degree resulted in a complete halt of protein release. Then, a lower amount of crosslinker was added, which resulted in a quick release in reducing buffer (Figure 4.5). The final molar ratio of protein:crosslinker used was 1:2. All further studies were conducted with the lower amount of crosslinker. After crosslinking, the Cyt c nanoparticles were centrifuged, washed with water, and lyophilized.

The protein nanoparticles were subsequently decorated with activated Ce6 through EDC chemistry (Figure 4.6). This results in non-cleavable amide bonds between the protein's lysine residues and the Ce6. The Ce6 modification was performed with two protein:drug molar ratios: 1:3 and 2:1. The purification process to remove the non-covalently immobilized Ce6 included the use of a centrifugal filter device. It allows for the physical separation of the Ce6 from the Cyt c prior to Ce6 quantification by measuring its absorbance at 400 nm. This is important, given the similarities in the absorption spectra of Cyt c and Ce6 (view Figure 4.7).

4.2.2 Protein residual activity and structure integrity retention after NP formulation

The pro apoptotic activity of Cyt c depends on its ability to reach the cytoplasm and interact with Apaf-1 to form the apoptosome. This in turn activates a caspase cascade that results in apoptosis. The caspase-3 activation by the synthesized bioconjugate NP was evaluated *in vitro*. Caspase-3 is an effector caspase that is at a meeting point of different signaling pathways leading to the cell entrance to apoptosis.

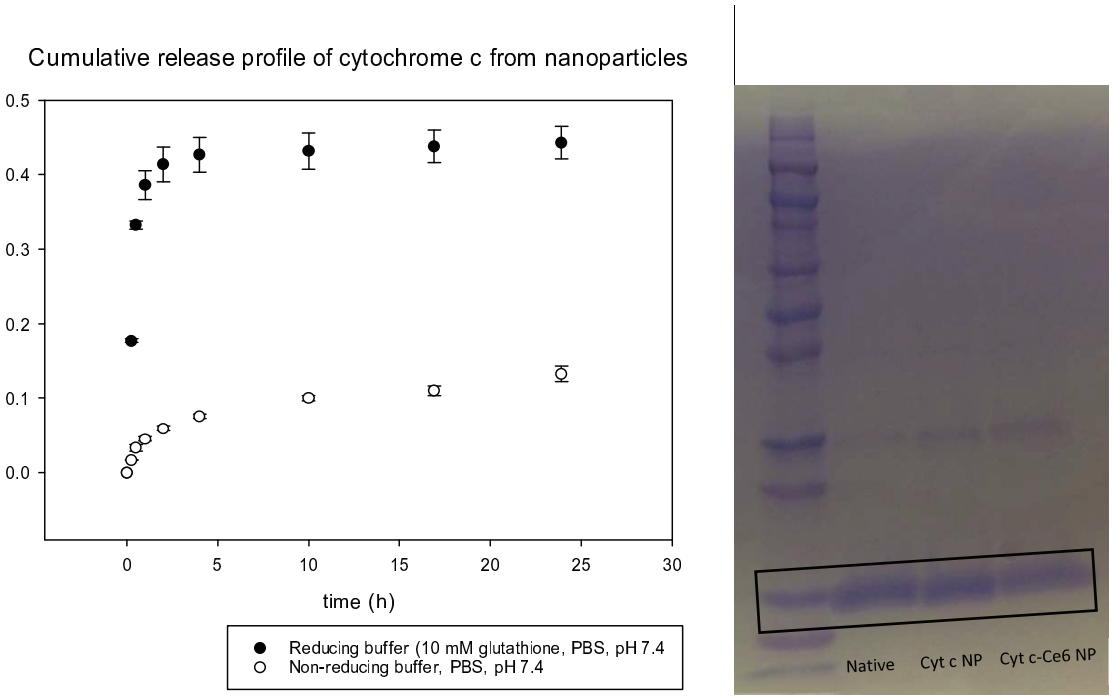

Figure 4.5 Left: Release profile of Cyt c NP crosslinked with a low amount of DSP. The Cyt c is effectively released in a reducing buffer (PBS containing 10 mM glutathione) within the first 3 hours, but is not readily released in regular PBS. Right: Reducing SDS-Polyacrylamide gel electrophoresis of Cyt c and Cyt c-Ce6 nanoparticles. Upon incubation of the nanoparticles in reducing conditions, the nanoparticles dissolved into protein monomers, as can be observed by the prominent band at approximately 12 kDa.

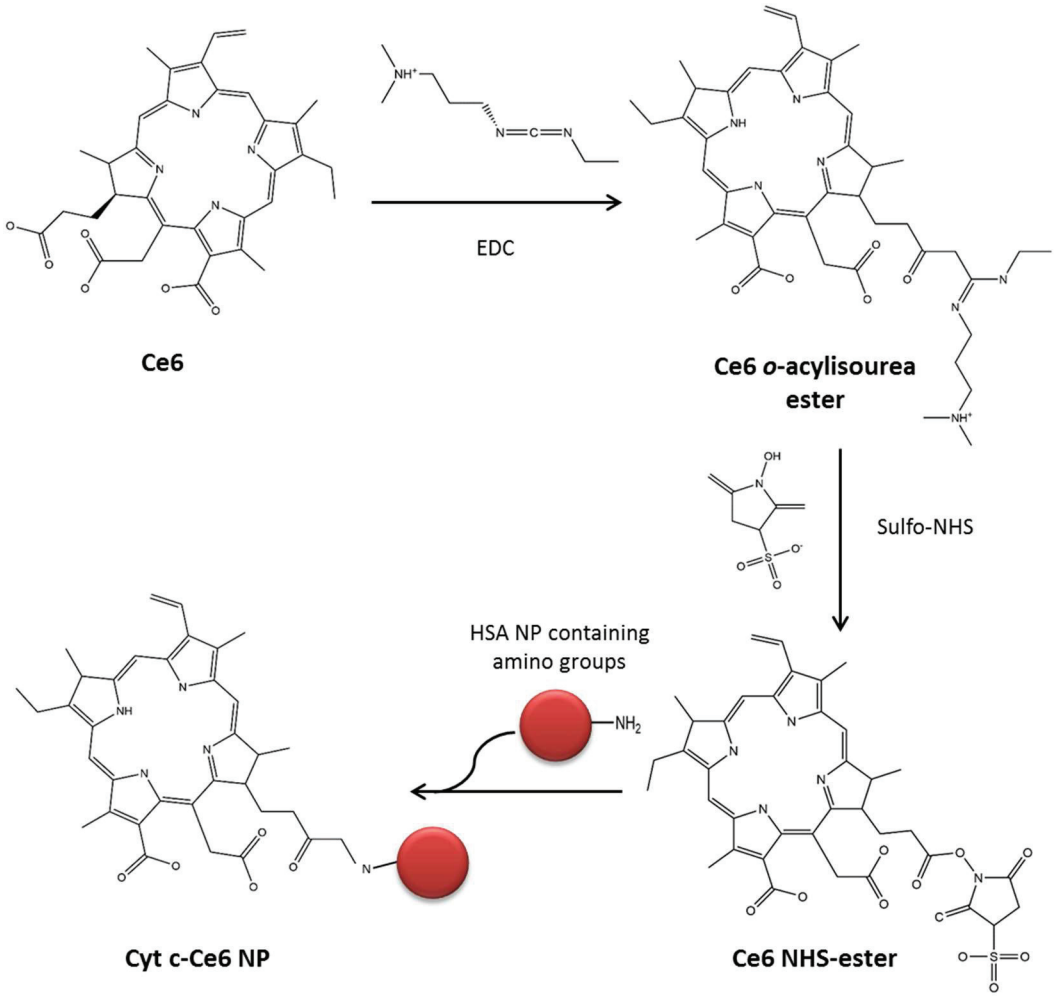

Figure 4.6 Reaction to activate Ce6 for its immobilization on the Cyt c lysines available on the nanoparticle surface through EDC/NHS chemistry.

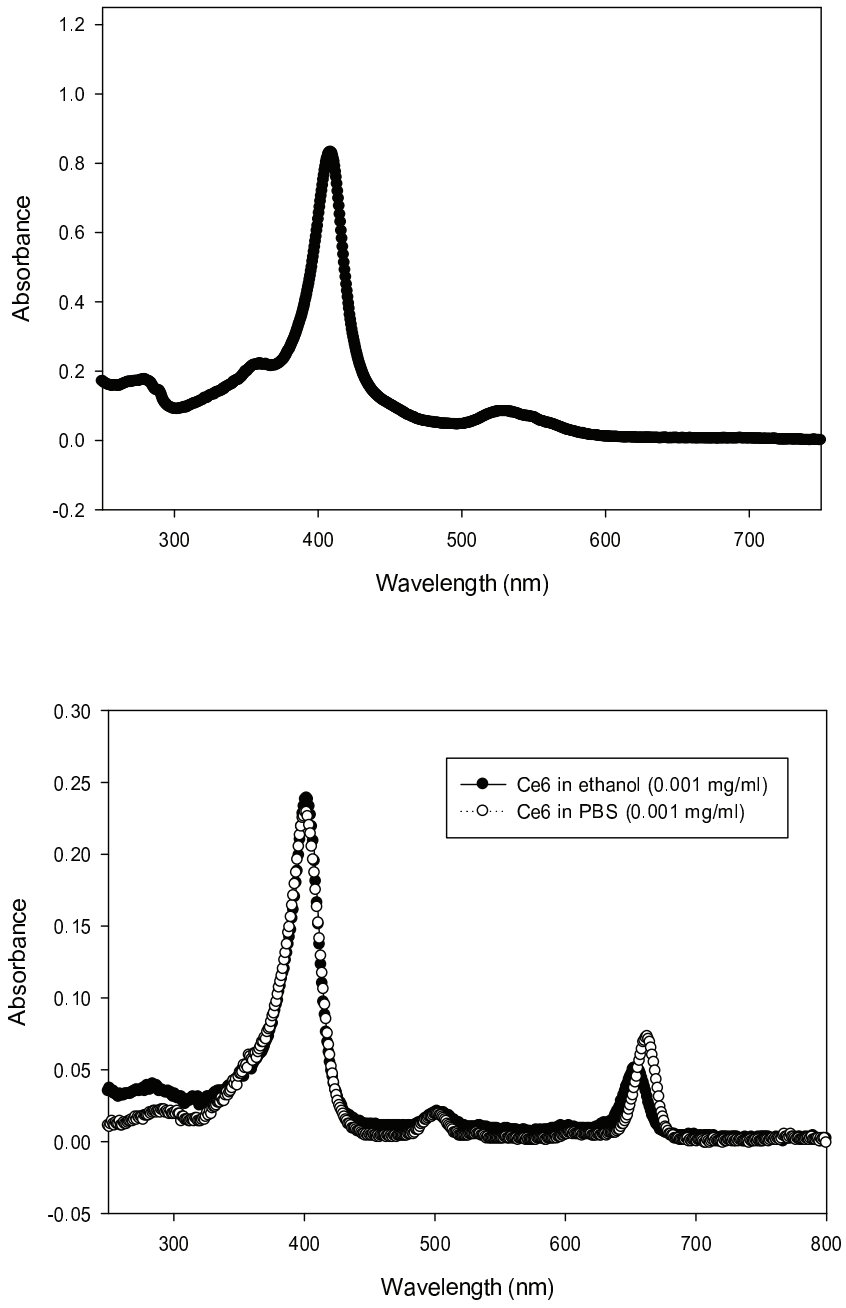

Figure 4.7 UV/Vis Absorbance spectra of Cyt c at 0.1 mg/ml (A), and free Ce6 dissolved in either PBS or ethanol at 0.001 mg/ml.

The synthesized Cyt c and Cyt c-Ce6 NP were incubated with the cells at a protein concentration of 75 μg/ml for 6 hours to allow for cell internalization. After incubation, lysis buffer and caspase-3 substrate was added. At this point, the membrane impermeable native Cyt c was added as a positive control. The Cyt c formulated into NP and crosslinked with DSP retained all of its activity, meaning that the exposure to acetonitrile during desolvation and crosslinking did not affect the protein activity. However, the immobilization of Ce6 at a protein:drug molar ratio of 1:3 affected its ability to activate caspase-3, lowering it by 66%. With a lower protein:drug molar ratio, the activity was mostly retained, and the Cyt c had a residual activity of 89% (Figure 4.8).

The decrease in activity may be explained by the changes in the protein structure that could potentially affect its interaction with Apaf-1 in the cytoplasm. To determine the structural changes induced in the Cyt c as a result of its formulation into nanoparticles with subsequent crosslinking and immobilization of Ce6 on the protein nanoparticle surface, circular dischroism (CD) spectroscopy was measured. CD spectroscopy is a technique that measures the differences in absorbance of left-hand and right-hand polarized light by chiral molecules, a property known as ellipticity. The secondary structures of proteins (α-helix, ß-sheet, and turns) can be studied by far-UV CD (200-250 nm), and their tertiary structure can be studied by near-UV CD (250-320 nm). Structural information for heme containing proteins can be also obtained near 410 nm (Ranjbar and Gill, 2009). Cyt c has an all-α far-UV CD spectrum, with characteristics negative bands at 208 nm (π–π* transition) and 222 nm (n–π* transition). Its near-UV spectra show bands

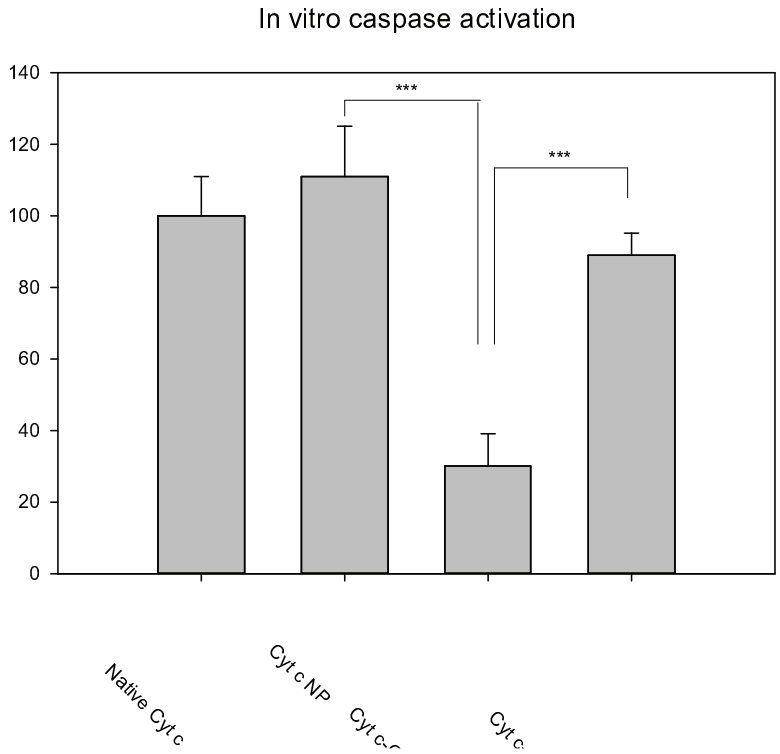

Figure 4.8 Caspase-3 activation of by Cyt c NP and Cyt c-Ce6 NP with two different drug ratios, corrected with the caspase-3 activation by native Cyt c.

for Tyr, Phe, and Trp residues that maintain tertiary structure by hydrophobic forces [Bharmonia et al., 2015].

Figure 4.9 shows the CD spectra of the Cyt c NP released from the Cyt c-Ce6 nanoparticles compared with the native Cyt c. In general, both the secondary and the tertiary structures are affected. The loss in definition of the peaks in the near-UV region accounts for differences in the environment of the hydrophobic residues, possibly to changes in protein folding. It is possible that some of the Cyt c, most likely in the outer part of the nanoparticle, completely loses its structure, while some retain it. This may explain the observed differences in CD spectra and the caspase-3 activation results.

However, the folding of Cyt c alone does not determine its binding to Apaf-1. The proposed binding of Cyt c to Apaf-1 takes place between the two tryptophan (W) and aspartate (D)-rich WD domains the WD-40 region of Apaf-1, which leads to a change in conformation an oligomerization to form the apoptosome [Chalaeva et al., 2015]. The electrostatic interactions between the positive charges near the heme edge are considered the most important factors in the Cyt c-Apaf-1 binding [Purrigh-Koch and MnLendon, 2000]. The most important role was played by Lys72, but additional 9 lysine residues has been described to have a role in the apoptosome formation [Kluck et al., 2000; Chandra et al., 2006]. The modifications of the lysine residues is most likely the key factor in the observed decrease in Cyt c activity.

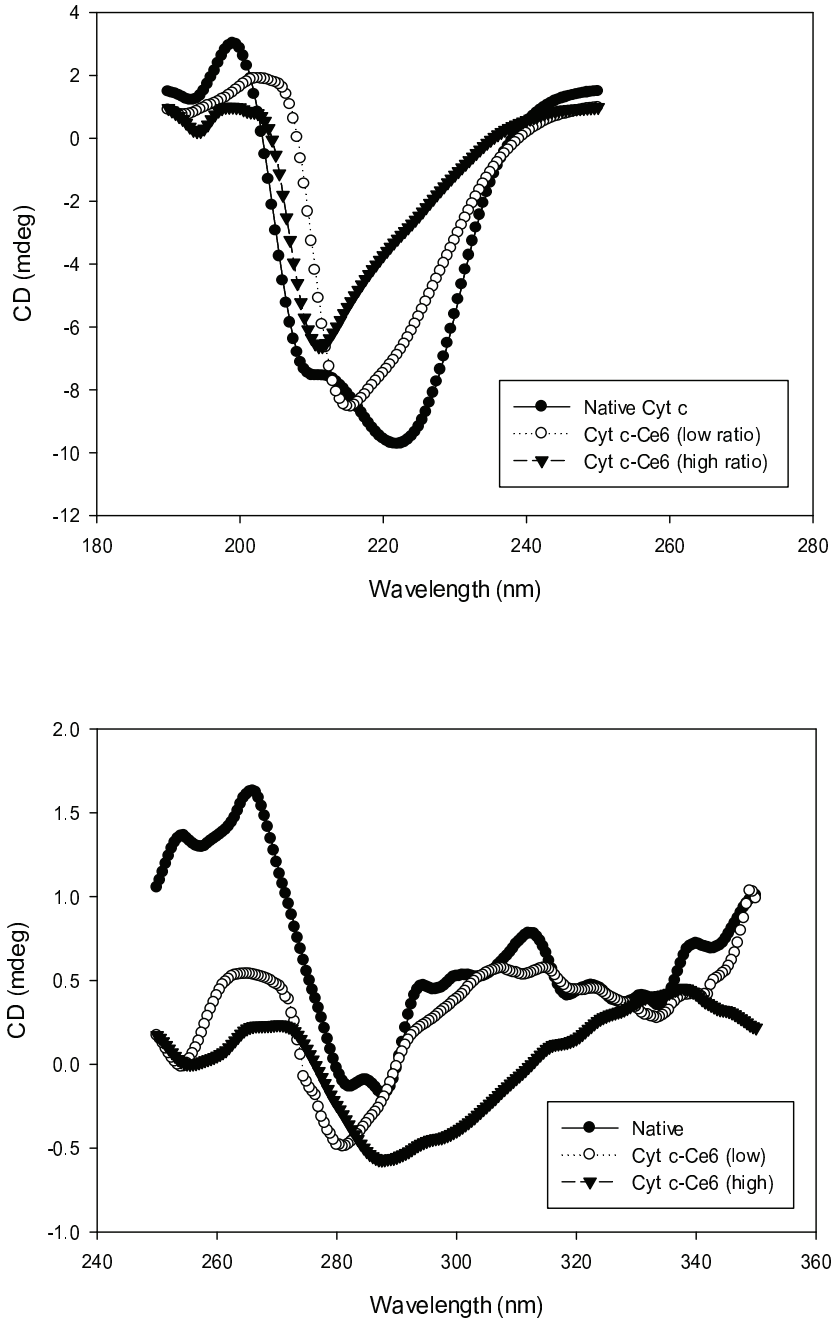

Figure 4.9 Far-UV (190-250 nm) and near-UV (250-350 nm) CD spectra showing the secondary and tertiary structures of Cyt c, respectively.

4.2.3 Cell internalization and cytotoxicity induced by Cyt-Ce6 nanoparticles

Cell internalization of Cyt c nanoparticles was evaluated by confocal microscopy. FITC-labeled Cyt c and Cyt c-Ce6 nps (low ratio) were incubated with HeLa cells for 6 hours at a protein concentration of 75 µg/ml. Native Cyt c was used as a control. The results show that, as expected, the native protein cannot penetrate the plasma membrane to localize in the cell cytoplasm. However, the formulation of Cyt c into nanoparticles allow for cell uptake after 6 hours. The Cyt c-Ce6 nanoparticle are effectively internalized as well (Figure 4.10). We show here that, in cell culture monolayers, nanoparticles are internalized even without having a ligand targeting a cell surface receptor. The nanoparticles are probably internalized by micropinocytosis [Kettler et al., 2014]. Even though we would not expect to observe this behavior in vivo, this strategy can potentially help researchers transport membrane impermeable proteins across the plasma membrane to study their intracellular effect without the use of mechanical methods, such as electroporation and microinjection.

Next, we studied the cell death induction of HeLa cells by the synthesized Cyt c-Ce6 nanoparticles (Figure 4.11). The cell death was quantitatively determined by the MTS colorimetric method, which measures the formation of formazan by metabolically active cells. This assay can quantitate the cells that were killed by the treatment, but cannot distinguish between apoptotic and necrotic cells. The results show that, at the concentrations tested, the native Cyt c cannot induce cell death. However, Cyt c formulated into redox-responsive nanoparticles effectively induces cell death in a dose

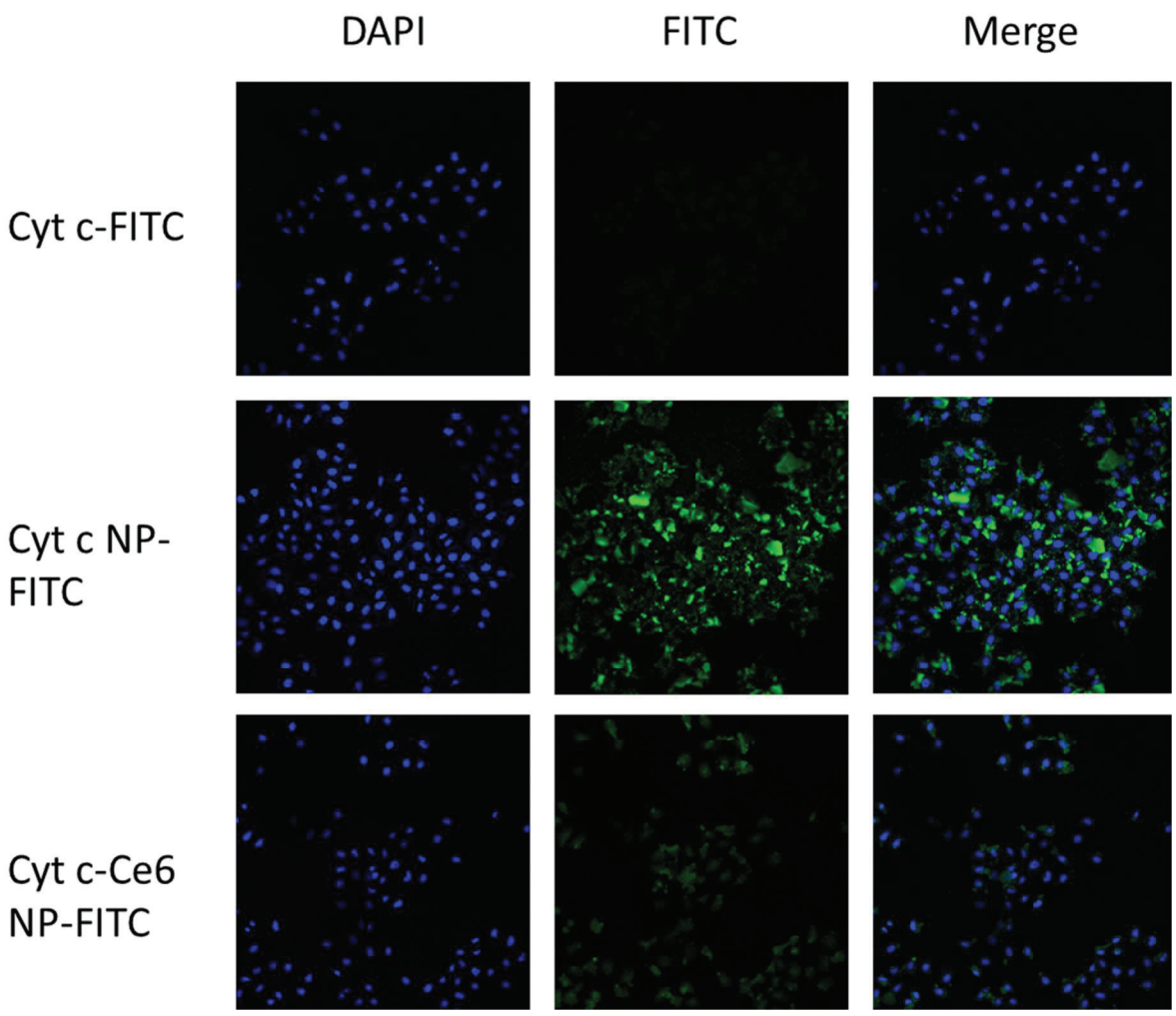

Figure 4.10 NP uptake by HeLa cells. After 6 hours of incubation with either FITC-labeled native Cyt c, Cyt c NP, and Cyt c-Ce6 NP, the cells were stained with DAPI and fixed for their examination by confocal laser scanning microscopy. The impermeable native Cyt c did not enter the cell. However, the Cyt c formulated into NP was internalized, even in the absence of a ligand targeting a cell surface receptor.

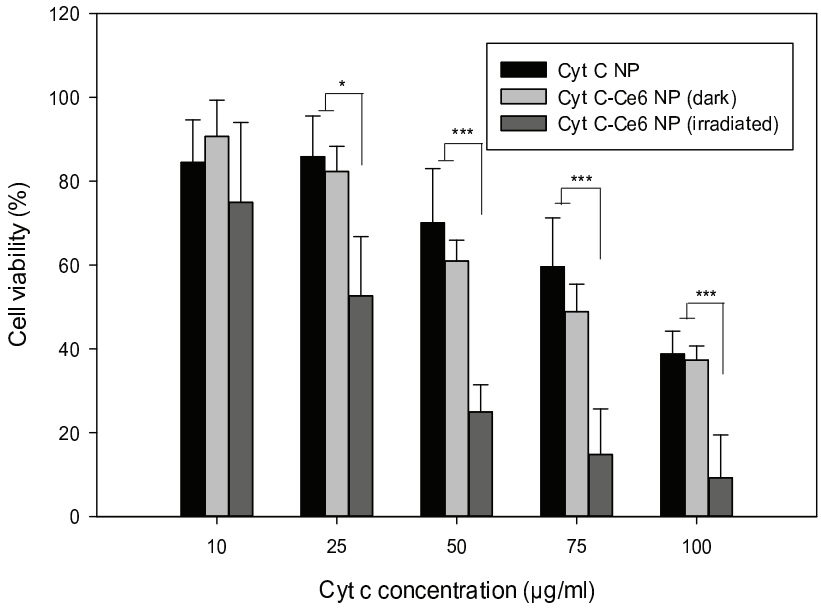

Figure 4.11 Cell viability assay of HeLa cells incubated with different concentrations of Cyt c nanoparticle and Cyt c-Ce6 nanoparticles both dark and irradiated. Asterisks indicate statistical significance with *p<0.05, and ***p<0.0001.

responsive manner. We compared the dose-dependent cell death induction of the Cyt c-Ce6 nanopaticles (low ratio) at each corresponding protein concentration, both in dark conditions and after irradiation. The concentration of Ce6 in the nanoparticles is approximately 0.025 mg/mg nanoparticles. In other words, there are 2.5 μg of Ce6 in 100 μg of Cyt c, or an approximate 2:1 protein:drug ratio. A low Ce6 concentration together with a low irradiation fluence rate was applied to cells to favor apoptosis over necrosis. The light flux applied was 1 J/cm^2. The results show that the low-dose PDT with Ce6 significantly increases the total cytotoxicity induce by the Cyt c nanoparticles at concentrations of 1.25-2.5 μg/ml. In accordance with the literature, it is possible that the increased production of ROS in the cell triggers the intrinsic apoptotic pathway, enhancing the cytotoxic activity of the delivery system [Green and Reed, 1998; Orrenius et al., 2007].

The cell death mechanism induced by the synthesized system was investigated next. Apoptosis induction was evaluated by Annexin V/PI staining followed by confocal microscopy examination. Annexin V conjugated to green fluorescent FITC detects the externalization of phosphatidylserine in apoptotic cells. Propidium iodide (PI) stains necrotic, or vary late apoptotic cells with red fluorescence. After incubation with the systems at 75 μg/ml for 6 hours in dark conditions, the cells were stained with both probes. As a result, apoptotic cells exhibit green fluorescence, dead cells show red and green fluorescence, and live cells show little or no fluorescence. Figure 4.12 shows that the native Cyt c and free Ce6 (no irradiation) do not induce apoptosis or cell death at the concentrations tested. However, both the Cyt c nanoparticles and the Cyt c-Ce6 nanopar-

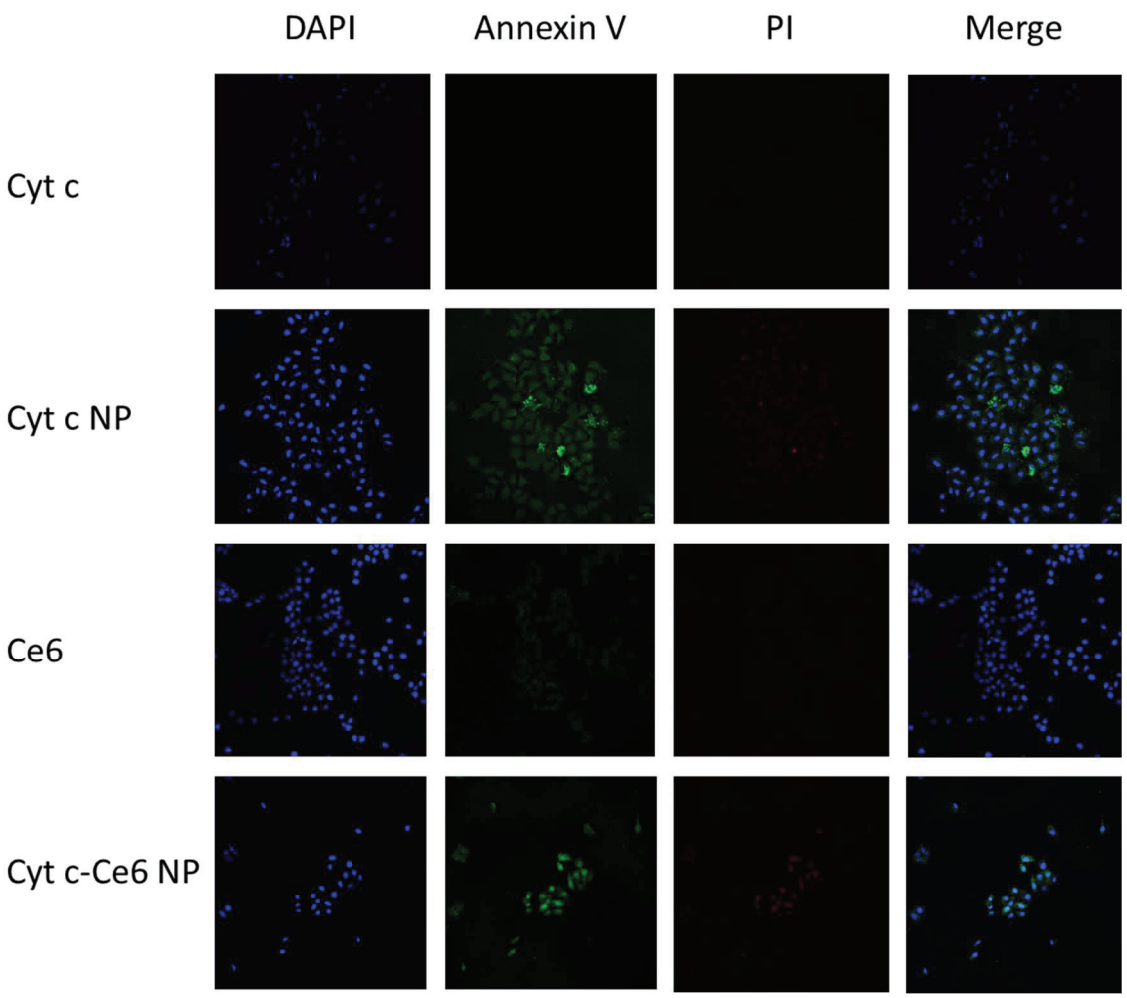

Figure 4.12 Examination of cell death mechanism induced by the Cyt c and the Cyt c-Ce6 nanoparticles. Annexin V conjugated to green-fluorescent FITC dye detects the externalization of phosphatidylserine in apoptotic cells, characteristic of apoptotic cells. Propidium iodide (PI) is a non-permeable dye that stains necrotic or late apoptotic cells, which have lost its plasma membrane integrity, with red fluorescence. After treatment with both probes, apoptotic cells show green fluorescence, dead cells show both red and green fluorescence, and live cells show little or no fluorescence.

ticles induce apoptosis. This is additional evidence that the Cyt c formulated into nanoparticles can effectively induce apoptosis.

The cell induction by necrosis was determined by an assay that studies the cell membrane integrity. It measures the release of lactate dehydrogenase (LDH), a stable cytoplasmic enzyme that is rapidly released as a result of membrane damage. The results show that, at the tested concentrations, neither the free Ce6 nor the immobilized Ce6 produce significantly different amounts of membrane damage related to necrotic cell death (Figure 4.13). This results indicate that the cell death induced by our system is mainly apoptosis, and that the increase in cell death as the result of the combination of the Cyt c with the Ce6 is not a result of necrosis induction.

4.3 Conclusions

We successfully designed a redox sensitive delivery system that co-delivers a protein and a photosensitizer drug intracellularly, increasing the overall therapeutic index of the protein nanoparticle. The desolvation method was used to obtain Cyt c nanoparticles (NP) The NP surface was then decorated with Ce6. Our previous study showed that the Ce6 can be reversibly photoquenched by immobilization on a protein NP, and its photodynamic activity can be recovered upon protein dissolution. Our drug and protein delivery NP effectively broke down in an environment emulating the reducing intracellular environment with 10 mM glutathione, but not significantly under extracellular conditions. The protein structure and function preservation after protein modification and formulation into a NP was evaluated. The caspase activation, an indica-

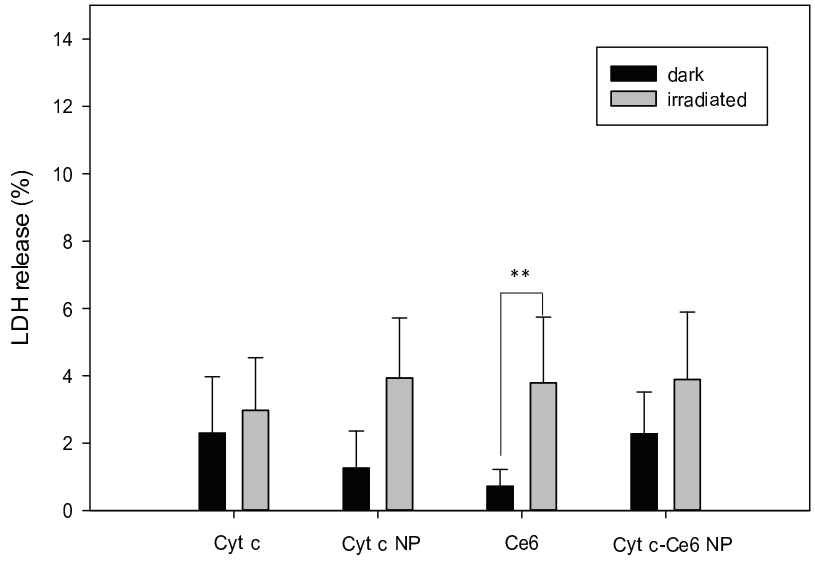

Figure 4.13 Membrane integrity assay to evaluate the induction of necrosis by the synthesized Cyt c-Ce6 nanoparticles. After incubation of the HeLa cells with native Cyt c, Cyt c nanoparticles, Cyt c-Ce6 nanoparticles, and free Ce6 for 6 hours, the cells were irradiated. Cell kept in the dark and untreated cells were used as controls. The lysed cells were used as a positive control. Asterisk indicate statistical significance with **$p<0.001$.

tor of the protein function, was found to be affected by the covalent immobilization of the Ce6, but the combination of both therapeutic agents into a single DDS increased the amount of cells killed by up to 45%. For the first time, a Cyt c-Ce6 redox-responsive nanoparticle drug delivery system has been designed and tested for cancer treatment. This research provides a means of designing more efficient cancer treatments.

The mild protein modification is necessary for the protein to retain its structure and function. The delivery system acts by inducing cell death by two independent pathways, providing a new means to sidestep multidrug resistance. The same rationale can be used to co-deliver other protein drug combinations and provides a model for future personalized medicine applications.

We have also shown that protein nanoparticles are internalized by cells *in vitro* without the need of a targeting moiety. The protein formulation into a dissolvable nanoparticle can help researchers investigate the protein's function inside of the cell without the use of mechanical methods, such as electroporation and microinjection.

Future work to improve the designed system includes the addition of a targeting mechanism to improve cell internalization *in vitro* and allow for targeted cell uptake *in vivo.* Additional surface modifications can also be incorporated to enhance circulation times *in vivo*. Moreover, further studies are needed in order to definitely determine the cellular pathways that lead to increased apoptosis induction as a result of the combinationn of Cyt c and Ce6 into a single delivery system.

4.4. Bibliography

Almeida, R.D.; Manadas, B.J.; Carvalho, A.P.; Duarte, C.B. Intracellular signaling mechanisms in photodynamic therapy. *Biochim. Biophys. Acta*. **2004**, *1704*, 59–86.

Bharmoria, P.; Trivedi, T.J.; Pabbathi, A.; Samantac, A.; Kumar, A. Ionic liquid-induced all-a to a + b conformational transition in cytochrome c with improved peroxidase activity in aqueous medium. *Phys. Chem. Chem. Phys.* **2015**, *17*, 10189.

Cai, J.; Yang, J.; Jones, D.P. Mitochondrial control of apoptosis: the role of cytochrome c. *Biochim. Biophys. Acta – Bioenergetics*. **1998**, *1366*, 139–149.

Chandra, D.; Bratton, S.B.; Person, M.D.; Tian, Y.; Martin, A.G.; Ayres, M.; et al. Intracellular nucleotides act as critical prosurvival factors by binding to cytochrome C and inhibiting apoptosome. *Cell*. **2006**, *125*, 1333–1346.

Frei, E. III; Eder J.P. Combination Chemotherapy. In *Holland-Frei Cancer Medicine*, 6th edition; Kufe D. W., Ed.; BC Decker: Hamilton, 2003.

Fu, A.; Tang, R.; Hardie, J.; Farkas, M.E.; Rotello, V.M. Promises and Pitfalls of Intracellular Delivery of Proteins. *Bioconjugate Chem*. **2014**, *25*, 1602−1608.

Ghavami G, Kazemali MR, Sardari S. Informatics of drug synergism in naturally occurring anticancer agents. *Recent Pat. Anticancer Drug Discov*. **2011**, 1, 26-44.

Green, D.R.; Reed, J.C. Mitochondria and apoptosis. *Science*. **1998**, *281*, 1309–1312.

Holoch, P.A.; Griffith, T.S. TNF-related apoptosis-inducing ligand (TRAIL): a new path to anti-cancer therapies. *Eur. J. Pharmacol*. **2009**, *625*, 63–72.

Jiang, T.; Mo, R.; Bellotti, A.; Zhou, J.; Gu, Z., Gel–Liposome-Mediated Co-Delivery of Anticancer Membrane-Associated Proteins and Small-Molecule Drugs for Enhanced Therapeutic Efficacy. *Adv. Funct. Mater*. **2014**, *24*, 2295–2304.

Kettler, K.; Veltman, K.; van de Meent, D.; van Wezel, A.; Hendriks, A.J. Cellular uptake of nanoparticles as determined by particle properties, experimental conditions, and cell type. *Env. Toxicol. Chem*. **2014**, *33*, 1552-8618.

Kluck, R.M.; Ellerby, L.M.; Ellerby, H.M.; Naiem, S.; Yaffe, M.P.; Margoliash, E.; Bredesen, D.; Mauk, A.G.; Sherman, F.; Newmeyer, D.D. Determinants of cytochrome c pro-apoptotic activity. The role of lysine 72 trimethylation. *J. Biol. Chem*. **2000**, *275*, 16127-16133.

Mendez, J.; Morales-Cruz, M.; Delgado, Y.; Figueroa, C.M.; Orellano, E.A., Morales, M., Monteagudo, A., Griebenow, K. Delivery of chemically glycosylated cytochrome c immobilized in mesoporous silica nanoparticles induces apoptosis in HeLa cancer cells. *Mol. Pharmacol*. **2014**, *11*, 102–111.

Mojzisova, H.; Bonneau, S.; Vever-Bizet, C.; Brault, D. Cellular uptake and subcellular distribution of chlorin e6 as functions of pH and interactions with membranes and lipoproteins. *Biochim. Biophys. Acta – Biomembranes*. **2007**, *1768*, 2748–2756.

Molina, A. M.; Morales-Cruz, M.; Benítez, M.; Berríos, K.; Figueroa, C. M.; Griebenow, K. Redox-sensitive cross-linking enhances albumin nanoparticle function as delivery system for photodynamic cancer therapy. *J. Nanomed. Nanotech*. **2016**, *6*, 294.

Morales-Cruz, M.; Figueroa, C.M.; González-Robles, T.; Delgado, Y.; Molina, A.; Méndez, J.; Morales, M.; Griebenow, K. Activation of caspase-dependent apoptosis by intracellular delivery of Cytochrome c-based nanoparticles. *J. Nanobiotechnol*. **2014**, *12*, 33.

Morales-Cruz, M.; Cruz-Montañez, A.; Figueroa, C.; Gonzalez-Robles, T.; Davila, J.; Inyushin, M.; Loza-Rosas, S.; Molina, A.; Muñoz-Perez, L.; Kucheryavykh, L.; Tinoco, A.; Griebenow, K. Combining stimulus-triggered release and active targeting strategies improves cytotoxicity of cytochrome c nanoparticles in tumor cells. *Mol. Pharm*. **2016**

Ng, D. Y. W.; Fahrer, J.; Wu, Y.; Eisele, K.; Kuan, S. L.; Barth, H.; Weil, T. Efficient Delivery of p53 and Cytochrome C by Supramolecular Assembly of a Dendritic Multi-Domain Delivery System. *Adv. Health. Mat*. **2013**, 2, 1620–1629.

Orrenius, S.; Gogvadze, V.; Zhivotovsky, B. Mitochondrial oxidative stress: implications for cell death. *Annu. Rev. Pharmacol. Toxicol*. **2007**, *47*, 143–183.

Purring-Koch, C.; McLendon, G. Cytochrome c binding to Apaf-1: The effects of dATP and ionic strength. *PNAS*. **2000**, *97*, 11928–11931.

Santra, S.; Kaittanis, C.; Perez, J.M. Cytochrome c Encapsulating Theranostic Nanoparticles: A Novel Bifunctional System for Targeted Delivery of Therapeutic Membrane-Impermeable Proteins to Tumors and Imaging of Cancer Therapy. *Mol. Pharm.* **2010**, *7*, 1209-22.

Shalaeva, D. N.; Dibrova, D. V.; Galperin, M. Y.; Mulkidjanian, A. Y. Modeling of interaction between cytochrome c and the WD domains of Apaf-1: bifurcated salt bridges underlying apoptosome assembly. *Biol. Direct*. **2015**, *10*, 29.

Strickley, R. G. Solubilizing Excipients in Oral and Injectable Formulations. Pharm. Res. **2004**, *21*, 201-230.

Szliszka, E.; Czuba, Z.P.; Kawczyk-Krupka, A.; Sieron-Stoltny, K.; Sieron, A.; Krol, W. Chlorin-based photodynamic therapy enhances the effect of tumor necrosis factor-related apoptosis inducing ligand (TRAIL) in bladder cancer cells. *Med. Sci. Monit*. **2012**, *18*, 47-53.

Xu, J.; Wang, J.; Luft, J. C.; Tian, S.; Owens, G. J.; Pandya, A. A.; Berglund, P.; Pohlhaus, P.; Maynor, B. W.; Napier, M. E.; DeSimone, J. M. Rendering Protein-Based Particles Transiently Insoluble for Therapeutic Applications. *J. Am. Chem. Soc*. **2012**, *134*, 8774-8777.

Yeh, T.H.; Wu, F.L.; Shen, L.J. Intracellular delivery of cytochrome c by galactosylated albumin to hepatocarcinoma cells. *J. Drug Targ*. **2014**, *22*, 528-535.